Uncertainty contributions to low-flow projections in Austria

J. Parajka[1], A.P. Blaschke[1], G. Blöschl[1], K. Haslinger[2], G. Hepp[3], G., Laaha[4], W. Schöner[5], H. Trautvetter[3], A. Viglione[1] and M. Zessner[3]

[1]{Institute for Hydraulic and Water Resources Engineering, TU Wien, Vienna, Austria}

[2]{Climate Research Department, Central Institute for Meteorology and Geodynamics, Vienna, Austria}

[3]{Institute for Water Quality, Resource and Waste Management, TU Wien, Vienna, Austria}

[4]{Institute of Applied Statistics and Computing, University of Natural Resources and Life Sciences (BOKU), Vienna, Austria}

[5]{Department of Geography and Regional Science, University of Graz, Graz, Austria}

Correspondence to: J. Parajka (parajka@hydro.tuwien.ac.at)

Abstract

The main objective of the paper is to understand the contributions to the uncertainty in low-flow projections resulting from hydrological model uncertainty and climate projection uncertainty. Model uncertainty is quantified by different parameterizations of a conceptual semi-distributed hydrologic model (TUWmodel) using 11 objective functions in three different decades (1976-86, 1987-97, 1998-08), which allows disentangling the effect of the objective function-related uncertainty and temporal stability of model parameters. Climate projection uncertainty is quantified by four future climate scenarios (ECHAM5-A1B, A2, B1 and HADCM3-A1B) using a delta change approach. The approach is tested for 262 basins in Austria.

The results indicate that the seasonality of the low-flow regime is an important factor affecting the performance of model calibration in the reference period and the uncertainty of Q_{95} low-flow projections in the future period. In Austria, the range of simulated Q_{95} in the reference period is larger in basins with summer low-flow regime than in basins with winter

low-flow regime. Using different calibration periods may result in a range of up to 60% in simulated Q_{95} low flows.

The low-flow projections of Q_{95} show an increase of low flows in the Alps, typically in the range of 10-30% and a decrease in the south-eastern part of Austria mostly in the range -5 to -20% for the climate change projected for future period 2021-50 relative the reference period 1978-2007. The change in seasonality varies between scenarios, but there is a tendency for earlier low flows in the Northern Alps and later low flows in Eastern Austria. The total uncertainty of Q_{95} projections is the largest in basins with winter low-flow regime and, in some basins it exceeds 60%. In basins with summer low flows, the total uncertainty is mostly less than 20%. The ANOVA assessment of the relative contribution of the three main variance components (i.e. climate scenario, decade used for model calibration and calibration variant representing different objective function) to the low-flow projection uncertainty shows that in basins with summer low-flows the climate scenarios contribute more than 75% to the total projection uncertainty. In basins with winter regime, the median contribution of climate scenario, decade and objective function is 29%, 13% and 13%. While the objective function-related uncertainty dominates over climate projection uncertainty in terms of low-flow magnitudes, the opposite is the case for low-flow seasonality. The implications of the uncertainties identified in this paper for water resources management are discussed.

1 Introduction

Understanding climate impacts on hydrologic water balance in general and extreme flows in particular is one of the main scientific interests in hydrology. Stream flow estimation during low-flow conditions is important also for a wide range of practical applications, including estimation of environmental flows, effluent water quality, hydropower operations, water supply or navigation. Projections of low flows in future climate conditions are thus essential for planning and development of adaptation strategies in water resources management. However it is rarely clear how the uncertainties in assumptions used in the projections translate into uncertainty of estimated future low flows.

There are numerous regional and national studies that have analyzed the effects of climate change on the stream flow regime, including low flows (e.g. Feyen and Dankers, 2009, Prudhomme and Davies, 2009, Chauveau et al., 2013 among others). Most of them apply outputs from different global or regional climate circulation models, which are based on

different emission scenarios. The projections of low flows are then typically simulated by hydrologic models of various complexity. There is an increasing number of studies evaluating different sources of uncertainty in river flow projections resulting from different GCMs, downscaling methods or hydrologic model parametrization (e.g. Dobler et al., 2012, Finger et al., 2012, Coron et al., 2012, Addor et al., 2014, Chiew et al., 2015). Only few studies, however, evaluate the uncertainty of low-flow projections and the relative contribution of its different sources (i.e. climate projection, hydrologic model structure and/or model parameterizations). Such studies include assessment of the impact of different climate projections on low flows evaluated e.g. in Huang et al. (2013) and Forzieri et al. (2014). While Huang et al. (2013) assesses the low-flow changes and uncertainty in the five largest river basins in Germany, Forzieri et al. (2014) evaluates the uncertainty of an ensemble of 12 bias corrected climate projections in the whole of Europe. Both studies quantify uncertainty in terms of the number of low-flow projections that suggest the same change direction. Their results indicate a consistent pattern of low-flow changes across different regions in Europe. A common feature of such ensemble climate scenarios is an increase in the agreement between ensemble members with increasing future time horizon of climate projections. The impact of hydrologic model structure and climate projections was evaluated in Dams et al. (2015). They applied four hydrologic models calibrated with four objective functions to simulate the impact of three climate projections on low flows for a basin in Belgium. They found that besides the uncertainty introduced by climate change scenarios, hydrologic model selection introduces an additional considerable source of uncertainty in low-flow projections. The model structure uncertainty was particularly important under more extreme climate change scenarios. A similar study was performed by Najafi et al. (2011) who investigated the uncertainty stemming from four hydrologic models calibrated by three objective functions and applied on eight Global Climate Model (GCM) simulations in a basin in Oregon. Their results show that although in general the uncertainties from the hydrologic models are smaller than from GCM, in the summer low-flow season, is the impact of hydrologic model parametrization on overall uncertainty considerably larger than of the GCM.

The quantification of the relative contribution of different sources to the overall uncertainty of stream flow projections is recently evaluated by using analyses of variance (ANOVA) (Storch and Zwiers, 1999). Bosshard et al. (2013) synthetized previous studies that investigate hydrological climate-impact projections and their sensitivity to different uncertainty sources. They propose an ANOVA framework to separate the uncertainty from climate models,

statistical post-processing (bias correction and delta change approach) and hydrological models. Addor et al. (2014) use the ANOVA framework to quantify the uncertainty of stream flow projections resulting from the combination of emission scenarios, regional climate models, post-processing methods, and hydrological models of different complexity. They report that the main source of uncertainty stems from the climate models and natural climate variability, and the impact of emission scenario increases with increasing future time horizon of climate projections. Hingray and Said (2014) propose a quasi-ergodic two-way ANOVA framework for the partitioning of the total uncertainty of climate projections. This framework is recently tested for the estimation of climate and hydrological uncertainties of transient low flow projections in two basins in the southern French Alps (Vidal et al., 2015). The results show that a large part of the total uncertainty arises from the hydrological modelling and it can be even larger than the contribution from the GCMs.

The objective of this paper is to understand the relative contribution of the impact of hydrologic model calibration and ensemble climate scenarios to the overall uncertainty of low-flow projections in Austria. Here, the uncertainty and variability of low-flow projections is assessed for four climate scenarios, 11 variants of objective functions and three decades used for model calibration. Austria is chosen as a case study since it is an ideal test bed for such analysis, as it allows to disentangle the uncertainties separately in regions with summer and winter low-flow regimes. The assessment of uncertainties for winter and summer regimes allows to make generalisation for a similar spectrum of physiographic conditions around the world.

2 Methodology

2.1 Low-flow projections

In this study, low-flow projections of future climate scenarios are analysed by comparing future to past flows by using model forcing from a delta change approach. This concept allows to remove biases resulted from simulations when regional climate model (RCM) outputs are used as an input in hydrologic modelling. Instead of using RCM simulations of daily air temperature and precipitation for hydrologic model calibration, the model is first calibrated by using observed climate characteristics in the reference period. In a next step, RCM outputs are used to estimate monthly differences between simulations in the reference

(control) and future periods. These differences (delta changes) are then added to the observed model inputs and used for simulating future hydrologic changes. The daily precipitation is scaled by the relative monthly delta changes, with no change in the frequency of rainy days. The daily air temperature is changed by the absolute value of monthly delta changes. The differences between daily simulations of a hydrologic model in the reference and future periods are then used to interpret potential impacts of changing climate on future river flows.

The future low-flow changes are quantified by the Q_{95} low-flow quantile and seasonality index *SI*. The Q_{95} represents river flow that is exceeded on 95% of the days of the entire reference or future period. This characteristic is one of the low-flow reference characteristic which is widely used in Europe (Laaha and Blöschl, 2006). Seasonality index *SI* represents the average timing of low flows within a year (Laaha and Blöschl, 2006, 2007). It is estimated from the Julian dates D_j of all days when river flows are equal or below Q_{95} in the reference or future periods. *Dj* represents a cyclic variable. Its directional angle, in radians, is given by:

$$\theta_j = \frac{D_j \cdot 2\pi}{365} \tag{1}$$

The arithmetic mean of Cartesian coordinates x_θ and y_θ of a total of *n* single days *j* is defined as:

$$x_\theta = \frac{1}{n}\sum_j \cos(\theta_j) \tag{2}$$

$$y_\theta = \frac{1}{n}\sum_j \sin(\theta_j)$$

From this, the directional angle of the mean vector may be calculated by:

$$\theta = \arctan\left(\frac{y_\theta}{x_\theta}\right) \qquad 1^{st} \text{ and } 4^{th} \text{ quadrant: } x>0 \tag{3}$$

$$\theta = \arctan\left(\frac{y_\theta}{x_\theta}\right) + \pi \qquad 2^{nd} \text{ and } 3^{rd} \text{ quadrant: } x<0 \tag{4}$$

Finally, the mean day of occurrence is obtained from re-transformation to Julian Date:

$$SI = \theta \cdot \frac{365}{2\pi} \tag{5}$$

and the variability of the date of occurrence about the mean date (i.e. seasonality strength) is characterized by the length parameter *r*. The parameter *r* is estimated as (Burn, 1997):

$$r = \sqrt{\bar{x}^2 + \bar{y}^2} \Big/ n \quad (6)$$

and ranges from *r*=0 (low strength, uniform distribution around the year) to *r*=1 (maximum strength, all extreme events of floods occur on the same day).

The SI index is estimated for observed and simulated low flows. The differences between model simulations (i.e. Q_{95} and *SI* estimates) in the reference and future periods are then used to quantify potential impacts of climate change on low flows. Both Q_{95} and *SI* measures are estimated independently for the reference and future periods by the lfstat package in R software (Kofler and Laaha, 2014).

2.2 Hydrologic model

Low-flow projections are estimated by a conceptual semi-distributed rainfall-runoff model (TUWmodel, Viglione and Parajka, 2014). The model simulates water balance components on a daily time step by using precipitation, air temperature and potential evapotranspiration data as an input. The model consists of three modules which allow simulating changes in snow, soil storages and groundwater storages. The calibrated model parameters are presented in Table 1. More details about the model structure and examples of application in the past are given e.g. in Parajka et al. (2007, 2008), Viglione et al. (2013) and Ceola et al. (2015).

In this study, the TUWmodel is calibrated by using the SCE-UA automatic calibration procedure (Duan et al., 1992). The objective function (Z_Q) used in calibration is selected on the basis of prior analyses performed in different calibration studies in the study region (see e.g. Parajka and Blöschl, 2008, Merz et al., 2011). It consists of weighted average of two variants of Nash–Sutcliffe model efficiency, M_E and M_E^{log}. While the M_E efficiency emphasize the high flows, the M_E^{log} efficiency accentuates more the low flows. The maximized objective function Z_Q is defined then as

$$Z_Q = w_Q \cdot M_E + (1 - w_Q) \cdot M_E^{\log} \quad (7)$$

where w_Q represents the weight on high or low flows. If w_Q equals 1 then the model is calibrated to high flows, if it equals to 0 then to low flows only. M_E and M_E^{log} are estimated as

$$M_E = 1 - \frac{\sum_{i=1}^{n}\left(Q_{obs,i} - Q_{sim,i}\right)^2}{\sum_{i=1}^{n}\left(Q_{obs,i} - \overline{Q_{obs}}\right)^2} \quad (8)$$

$$M_E^{\log} = 1 - \frac{\sum_{i=1}^{n}\left(\log(Q_{obs,i}) - \log(Q_{sim,i})\right)^2}{\sum_{i=1}^{n}\left(\log(Q_{obs,i}) - \overline{\log(Q_{obs})}\right)^2} \quad (9)$$

where $Q_{sim,i}$ is the simulated discharge on day *i*, $Q_{obs,i}$ is the observed discharge, $\overline{Q_{obs}}$ is the average of the observed discharge over the calibration (or verification) period of *n* days.

2.3 Uncertainty estimation

The uncertainty, defined as the range of simulated low-flow indices, is evaluated for two contributions. The first analyses the uncertainty (i.e. the range of Q_{95} and *SI*) estimated for different variants of hydrologic model calibration. Here, two cases are evaluated. In order to assess the impact of time stability of model parameters (Merz et al., 2011), TUWmodel is calibrated separately for three different decades (1976-1986, 1987-1997, 1998-2008). The effect of objective functions used for the TUWmodel calibration is evaluated by comparing 11 variants of weights (w_Q) used in Z_Q. Following w_Q are tested: 0.0, 0.1, 0.2, 0.3, 0.4, 0.5, 0.6, 0.7, 0.8, 0.9 and 1.0. The hydrologic model is calibrated for all 11 variants in each selected decade. Calibrated models are then used for flow simulations and hence Q_{95} and *SI* estimation in the reference and future periods.

The second contribution evaluates the uncertainty of Q_{95} and *SI* changes simulated for different climate scenarios. The effect of calibration uncertainty (case 1) is compared for four selected climate scenarios (more details are given in Data section). The delta change approach is used to derive model forcing for selected future period and simulated future river flows are compared to model simulations in the reference period 1976-2008. The relative changes of Q_{95} and *SI* values between reference and future periods are estimated for four selected climate scenarios, 11 variants of model calibration and three selected decades. The relative contribution of the impact of model calibration (i.e. time stability and objective function selection) and climate scenario is evaluated seasonally at the regional scale.

The uncertainty of low flow projections is then compared to the range of low-flow indices obtained by different calibration variants in the reference period. In addition, the total uncertainty of future low flow projections is decomposed to individual components by means of analysis of variance (ANOVA; e.g. Hingray and Said, 2014; Lafaysse et al., 2014; Vidal et al, 2015; and von Storch and Zwiers, 1999, chap. 9 for a general introduction to ANOVA). The 3-way ANOVA approach is employed to decompose total uncertainty of the projected low-flow changes into three main variance components. These variance components represent uncertainty contributions of 3 main effects: climate scenario (factor A with $I = 4$ levels), decade used for model calibration (factor B with $J = 3$, levels) and calibration variant representing different objective functions (factor C with $K = 11$ levels). The ANOVA model is defined as follows:

$$\Delta Q95_{ijk} = \mu + \alpha_i + \beta_j + \gamma_k + \epsilon_{ijk} \quad (10)$$

In this linear equation (Eq.10), $\Delta Q95_{ijk}$ denotes the ensemble projected changes in Q_{95} for the future horizon at a gauge. It is modelled by a global mean μ and the mean effects (deviations of factor-means from the global mean) of climate scenario ($\alpha_i ; i = 1, \dots, I$), decade ($\beta_j ; j = 1, \dots, J$), and calibration variant ($\gamma_k ; k = 1, \dots, K$), and ϵ_{ijk} are the residual errors of the model. In an ANOVA framework, the total variability of $\Delta Q95_{ijk}$ is characterised by the total sum of squares SS_T, and is decomposed into additive variance components of individual effects:

$$S_T = SS_A + SS_B + SS_C + SS_E \quad (11)$$

The variance components of the main effects A, B, C are computed as follows:

$$SS_A = JK \sum_{i=1}^{I} (\bar{y}_{i..} - \bar{y}_{...})^2 \quad (12)$$

$$SS_B = IK \sum_{j=1}^{J} (\bar{y}_{.j.} - \bar{y}_{...})^2 \quad (13)$$

$$SS_C = IJ \sum_{k=1}^{K} (\bar{y}_{..k} - \bar{y}_{...})^2 \quad (14)$$

The variance component of the residuals representing the unexplained variance is:

$$SS_e = \sum_{i=1}^{I} \sum_{j=1}^{J} \sum_{k=1}^{K} (y_{ijk} - \bar{y}_{i..} - \bar{y}_{.j.} - \bar{y}_{..k} + \bar{y}_{...})^2 \quad (15)$$

Based on the SS_e,, an estimate of the variance contributions of each effect A,B,C is computed as:

$$\eta_A^2 = \frac{SS_A}{SS_T} \; ; \; \eta_B^2 = \frac{SS_B}{SS_T} \; ; \; \eta_C^2 = \frac{SS_C}{SS_T} \; ; \; \eta_e^2 = \frac{SS_e}{SS_T} \quad (16)$$

The measure eta-square is also termed the coefficient of determination R^2 (Von Storch and Zwiers, 1999). Eta-square tends to overestimate the variance explained by one factor and is therefore a biased estimate of the effect size. A less biased estimator is given by the measure ω^2:

$$\omega_A^2 = \frac{SS_A - df_A * MS_e}{SS_T + MS_e} \quad (17)$$

where df_A denotes the degrees of freedom of a factor (e.g. for factor A with I levels, $df_A = I - 1$), and $MS_e = SS_E/df_e$ is the residual mean square error. The quantity MS_e denotes the mean residual sum of squares. It is computed by

$$MS_e = SS_e/df_e \tag{18}$$

The measure omega-square is also termed the adjusted R^2, in analogy to the adjusted coefficient of determination of multiple regression. Note that the degrees of freedom of the error term df_e depend on the total number of effects in the ANOVA design. For 3-way ANOVA without interactions df_e is obtained by:

$$df_e = df_T - df_A - df_B - df_C = IJK - I - J - K + 2 \tag{19}$$

Clearly, the adjustment of effect size increases if the residual degrees of freedom are small, what is the case when overall sample size is small. Hence the difference between both measures of effect size will be negligible for designs with large df_e, as it is the case for our study. In our assessment, we will therefore only present ω^2 which is the more general measure of effect size at each catchment. A spatial synthesis of uncertainty contributions for summer and winter dominated basins is finally obtained from the distribution of variance components across basins falling into each low-flow regime group.

3 Data

Study region is Austria (Fig.1). Austria represents diverse climate and physiographic conditions of Central Europe, which are reflected in different hydrologic regimes (Gaál et al., 2012). The topography varies from 115 m a.s.l. in the lowlands to more than 3700 m a.s.l. in the Alps. Austria is located in a temperate climate zone influenced by the Atlantic, meridional south circulation and the continental weather systems of Europe. Mean annual air temperature

varies between -8°C to 10°C. The mean annual precipitation ranges from 550mm/year in the Danube lowlands, to more than 3000mm/year on the windward slopes of the Alps.

The analysis is based on daily river flow measurements at 262 gauges (Fig. 1). This dataset represents a subset of data used in Laaha and Blöschl (2006), which consists of gauges for which hydrographs are not seriously affected by abstractions and karst effects during the low-flow periods. Fig.1 shows two main low-flow regimes in Austria. While orange and red colours indicate 130 stations with dominant summer (June-November) low-flow occurrence, blue colour indicates 132 gauges with winter (December-May) flow minima. These two groups represent basins with distinct low-flow seasons, which are controlled by different hydrologic processes. While the winter flow minima in the mountains are controlled by freezing processes and snow storage, summer low flows occur during long-term persistent dry periods when evapotranspiration exceeds precipitation. The different low-flow generating processes, together with the hydro-climatic variety of the study area, gives rise to an enormous spatial complexity of low flows in Austria. The largest values occur in the Alps, with typical values ranging from 6 to 20 $l\ s^{-1}\ km^{-2}$. The lowest values occur in the east ranging from 0.02 to 8 $l\ s^{-1}\ km^{-2}$, although the spatial pattern is much more intricate.

Climate data used in hydrologic modeling consists of mean daily precipitation and air temperature measurements at 1091 and 212 climate stations in the period 1976-2008, respectively. Model inputs have been prepared by spatial interpolation and zonal averaging described in detail in previous modeling studies (please see e.g. Merz et al., 2011 or Parajka et al, 2007). These data serve as a basis for hydrologic model calibration and as a reference for future change simulations. Fig. 2 shows basin averages of mean annual air temperature, precipitation and runoff in the period 1976-2008. The two groups of basins (winter vs. summer low flow regimes) clearly differ in the climate regime. Basins with summer low flows are characterized by higher air temperatures, less precipitation and less runoff. The comparison of three different decades indicates that mean annual air temperatures have increased by 1^{o}C in the period 1976-2008. This increase is similar for both groups of basins. Interestingly, the mean annual precipitation has increased over the last three decades, which is likely compensated by increased evapotranspiration, as the mean annual runoff remains rather constant.

The regional climate model (RCM) scenarios used in this study are based on the results of the reclip.century project (Loibl et al., 2011). The ensemble climate projections are represented

by COSMO-CLM RCM runs forced by the ECHAM5 and HADCM3 global circulation models for three different IPCC emission scenarios (A1B, B1 and A2, Nakicenovic et al., 2000). These represent a large spread of different emission pathways from a "business as usual" scenario with prolonged greenhouse gas emissions (A2), a scenario with moderate decline of emissions after 2050 (A1B) and a scenario indicating considerably reduced emissions from now on (B1).

Table 2 summarizes the annual and seasonal differences (delta changes) of mean basin precipitation and air temperature between the future (2021-2050) and reference (1978-2007) periods. Table 2 indicates that the largest warming is obtained by simulations driven by HADCM3. The median of air temperature increase in summer exceeds 2^{o}C. In numerous basins, a small decrease in air temperature in winter is simulated by ECHAM5 A2 and B1 simulations. The changes in mean annual precipitation are within the range ±9 % in all selected basins. The increase tends to be larger in winter than in the summer period.

4 Results

4.1 Low-flow simulations and uncertainty in the reference period

The runoff model efficiency (Z_Q) in the three calibration periods obtained for different variants of the objective function is presented in Fig. 3. The results show that Z_Q is larger and thus runoff simulations are more accurate in basins with winter (blue colour) than summer low-flow minimum (red colour). Most of the basins with winter low-flow regime are situated in the alpine western and central part of Austria, where the runoff regime is snow dominated. Such a regime has stronger runoff seasonality (see e.g. Fig. 5 in Laaha et al, this issue) and less difference in rainfall regime, which allows to model rainfall–runoff process easier than in basins with rainfall-dominated runoff regime.. Z_Q increases with decreasing weight w_Q, which indicates that the runoff model performance likely tends to be better for low than high flows. The comparison of Z_Q in the three calibration periods indicates that the difference in model performance between basins with winter and summer low-flow regime is the largest in the period 1976-1986. While the Z_Q for basins with winter low regime is very similar in all three calibration periods, the Z_Q has an increasing tendency in basins with summer regime. For example, the median of Z_Q for w_Q=1.0 increases from 0.64 in the period 1976-1986 to 0.71 in

the period 1998-2008. This increase is likely related to increasing number of climate stations and data quality (Merz et al., 2009).

How the different calibration variants and periods translate into low-flow 95%- quantile Q_{95} and seasonality *SI* is examined in Fig. 4. The model calibrated for 11 year period is used to simulate daily flows in the entire reference period 1976-2008. The results show that the model calibrated in the period 1976-1986 significantly overestimates Q_{95} of the reference period particularly in basins with summer low-flow regime. The period 1976–1986 is characterized by lower air temperatures with less evapotranspiration and relatively higher runoff generation rates which translates into different soil moisture storage (FC model parameter) and runoff generation (BETA) model parameters. Such effects are consistent with findings of Merz et al., (2011). The hydrologic model applied to the entire reference period hence produces larger runoff contribution which tends to overestimate Q_{95} particularly in the warmer and drier parts of the reference period and drier and warmer parts of Austria. The overestimation is consistent for large range of w_Q (w_Q in the range 0.0-0.9) and the median of Q_{95} difference exceeds 20%. Also the scatter around the median is rather large, where 25% of the basins with the summer low-flow regime have Q_{95} differences larger than 35%. The simulated Q_{95} in basins with winter low flows fit closer to the observed estimates. The median is less than 10% for variants w_Q<1. Interestingly, the model simulations based on calibration periods 1987-1997 and 1998-2008 are much closer to the observed values. The results for both groups of basins are very similar and essentially unbiased in terms of 95% low-flow quantile. The exception is the calibration variant w_Q=1 that tends to underestimate Q_{95}. There are any significant differences between calibration to low-flow only (w_Q=0.0) and other weights, with exception of w_Q=1, which represents a typical calibration of using classical Nash-Sutcliffe coefficient.

The results of the seasonality estimation are presented in the bottom panels of Fig. 4. It is clear that this hydrologic model tends to estimate the low-flow period later. This shift is larger in basins with summer low-flow regimes. While the median of *SI* difference in basins with winter regime is around 10-12 days in the period 1976-1986 and increases to 12-19 days in the period 1998-2008, the median of *SI* difference in basins with summer low flows is in the range of 18-32 days. The scatter is, however, much larger for basins with summer regime. Here the model simulates the season of low-flow occurrence with more than 2 months shift (earlier or later) in almost 50% of the basins. A typical example of such shift is provided in Fig. 5. The periods with flows below 95% quantile are often very short and the timing of

simulated low flows does not fit well with these periods. In some cases there is also a difference in the length of observed and simulated low-flow periods. Some small rainfall-runoff events in the summer or autumn cause an interruption of the observed low-flow periods, but the model simulates a complete absorption of the precipitation event by the soil storage and hence a longer low-flow period.

The spatial pattern of the variability of Q_{95} estimation in the reference period 1976-2008 is presented in Fig. 6. Fig. 6 shows the range of differences between simulated and observed Q_{95} for the different calibration variants. Left panels show the range for model calibrations performed by the same objective function (i.e. top left panel - w_Q=0.5 and bottom left panel - w_Q=0.0) used for calibration in the three different calibration periods (1976-86, 1987-97, 1998-08). Contrary, right panels show the range of differences for one calibration period but between 11 variants of the objective function (w_Q) (i.e. top right panel -1976-1986, bottom right panel -1998-2008). The results indicate that the Q_{95} differences vary more between the different objective functions (right panels), however in many basins the range exceeds 60% even if the model is calibrated by one objective function but in the different calibration periods. As already indicated in Fig.4, the differences are larger in basins with summer low flows, particularly for variants calibrated in the period 1976-1986. For particular basins, the differences are not strongly related to the weight w_Q used in the calibration, with an exception of w_Q=1, which tends to have the largest difference to observed Q_{95}. Some examples of the model performance for individual basins are given in companion paper of Laaha et al. (this issue).

Spatial variability of the model variability in terms of low-flow seasonality is presented in Fig. 7. The results clearly indicate that basins with winter low-flow regime (i.e. situated in the Alps) vary significantly less for different calibration settings than the basins with summer low-flow regime. The range of differences is typically less than 14 days in the mountains, compared to more than 90 days in many basins with the summer regime.

The comparison of *SI* and Q_{95} ranges indicates that large *SI* variability does not systematically mean large variability in terms of Q_{95}. For example, a cluster of basins situated in the south-eastern part of Austria (Styria) has a large *SI* range of difference (i.e. more than 90 days) for 11 calibration variants in the period 1976-1986, but the variability in Q_{95} is less than 20% for this case. The same applies for the opposite case of small *SI* and large Q_{95} variability in the alpine basins.

4.2 Low-flow projections and uncertainty in the future period

Low-flow projections for selected climate scenarios and different calibration weights w_Q are presented in Fig. 8. Rather than to evaluate in detail the projections in terms of absolute values of low-flow changes, the main focus is to assess the range of possible changes caused by different scenarios and objective function used for model calibration. The results show projections based on model calibration in 1998-2008, but the results are almost identical with results for the other two calibration periods (i.e. the average difference is around 1%). Fig. 8 clearly shows the difference in projections for basins with summer and winter low-flow regime, particularly for Q_{95} changes. It is hence important to evaluate the projections and their variability separately for different regimes. The comparison of different scenarios indicates that they are similar in terms of projecting an increase of winter low flows and a tendency for no change or decreasing low flows in the summer period. The increase of winter Q_{95} slightly varies between climate scenarios and tends to increase for calibration variants with larger w_Q. The difference in median between w_Q<0.4 and w_Q>0.8 is approximately 9%. The projections of Q_{95} changes in basins with summer low flows have significantly smaller variability and do not depend on w_Q. The change in low-flow seasonality (Fig. 8, bottom panels) is less pronounced. The median of projections is around 5 and 10 days earlier than in the reference period for basins with summer and winter regime, respectively. Interestingly, the variability between basins and w_Q is significantly smaller than obtained for different calibration variants in the reference period (Fig. 4).

Examples of spatial patterns of low-flow projections are presented in Fig. 9 and 10. The projections of Q_{95} changes (Fig. 9) indicate an increase of low flows in the Alps, typically in the range of 10-30%. A decrease is simulated in south-eastern part of Austria (Styria) mostly in the range of -5 - -20%. The most spatially different projection is provided by the HADCM3 A1B climate scenario which simulates the strongest gradient between an increase of Q_{95} in the Alps in winter and a decrease in south-eastern part in summer. The change in the seasonality varies between the scenarios, but there is a tendency for earlier low flows in the Northern Alps and a shift to later occurrence of low flows in the Eastern Austria (Fig. 10). As already indicated in Fig. 8, the shift in seasonality is larger than one month only in a few basins.

Figure 9 and 10 show projections of lows flows for four climate scenarios, but only one variant of hydrologic model parameters. The evaluation of the impacts of different calibration variants on the variability of low-flow projections is presented in Fig. 11 and 12. These figures indicate the range of Q_{95} (Fig. 11) and the seasonality occurrence (Fig. 12) changes obtained by 11 calibration variants and three calibration periods. The range of Q_{95} changes is interestingly the largest in basins with the winter low-flow regime. In the Alps, the increase of Q_{95} is often in the range of 15% to more than 60%. On the other hand, the future Q_{95} estimates vary only slightly between the calibration variants in basins with the summer low flows. The change is less than 20% in most of the basins. The impact of the selection of objective function is, however, much larger for the estimation of the seasonality changes. Depending on the calibration variant, the change in seasonality can vary within more than 3 months, e.g. in the south-eastern part of Austria.

The total uncertainty of low-flow projections of Q_{95} and *SI* is presented in Fig. 13. While the top panels show the range of low-flow characteristics for all climate scenarios, calibration variants and periods, the bottom panels show the ratio between the uncertainty of future low-flow projections to the range of low-flow indices simulated in the reference period. The results show that the Q_{95} range is less than 25% in approximately one third of analyzed basins. On the other hand, 20% of basins have a range larger than 50%. These are the basins with the winter low-flow regime. The variability in the date of low-flow occurrence is less than three months in 40% of the basins. In almost 20% of the basins, however, it is larger than five months. The ratio between the range of projections to the range of calibration differences (bottom panels in Fig. 13 and Fig. 14) indicates that only in 15% of the cases the climate projection uncertainty of Q_{95} is larger than the range obtained in the calibration period. Most of these basins are situated in the mountains (mean basin elevation above 1000m a.s.l.) and have winter low-flow regime. The range of calibrated Q_{95} is larger in almost all basins with the summer low-flow regime, which are characterized by lower mean basin elevation and larger aridity. On the other hand, the climate projection uncertainty dominates for the low-flow seasonality and is more than three times larger in 50% of basins, particularly in the Alps. The *SI* projection uncertainty is only in 15% of the basins lower than the *SI* range obtained in the calibration period. The *SI* uncertainty ratio tends to be lower with increasing mean basin elevation and the basin area, but there is no apparent relationship with the aridity of the basins.

The relative contribution of the three main variance components (i.e. climate scenario, decade used for model calibration and calibration variant representing different objective function) to the overall uncertainty of future low-flow projections is evaluated in Fig. 15. Left and right panels show the distribution of ANOVA variance components for basins with winter (left panel) and summer (right panel) low-flow regime, respectively. The results indicate that the variability from climate scenarios has a dominant contribution to the overall projection uncertainty in basins with summer low-flow regime. While in basins with winter low-flows the median contribution of the three variance components is 29% (climate scenario), 13% (calibration decade) and 13% (objective function), in basins with summer low-flow regime is the median contribution from climate scenario larger than 76%.

5 Discussion and conclusions

The objective of the study is to explore the relative role of hydrologic model calibration and climate scenarios in the uncertainty of low-flow projections. While many previous studies simulate only the change in hydrologic regime or extreme characteristics due to changes in climate, in this study we focus on the quantification of the range of low-flow projections (i.e. uncertainty) due to differences in the objective function used in model calibration, temporal stability of model parameters and an ensemble of climate projections.

There are a number of studies that compare the uncertainty of projected runoff changes due to different model structure, objective function or GCM and emission scenarios. These studies found that the hydrologic model uncertainty tends to be considerably smaller than that from GCM or emission scenarios (Najafi et al., 2011, Prudhomme and Davies, 2009). Such results, however, refer to the seasonal or monthly runoff and are based on only a limited number of basins. The quantification of the uncertainty in low flows is still rather rare. Some studies (e.g. Huang et al., 2013 and Forzieri et al., 2014) evaluate the low-flow uncertainty in terms of the number of projections with the same change direction. They showed that the uncertainty is controlled mainly by the differences in emission scenarios and it decreases with increasing projection horizon. Our results indicate that, although the uncertainty from different climate scenarios is larger than 40% in many basins, the range of low-flow indices from model calibration can exceed 60%. This result particularly relates to the assessment of low-flow quantile changes.

Some recent low-flow studies suggest to more explicitly distinguish between the processes leading to low-flow situations (see e.g. Fleig et al., 2006, Laaha et al., 2006, Van Loon et al., 2015, Forzieri et al., 2014). Following this recommendation, we analyzed the effects of model calibration and climate scenarios separately for basins with dominant winter and summer low-flow regimes. Our results indicate that the calibration runoff efficiency in basins with winter low-flow regime is larger (more accurate), and varies between basins less than in basins with summer low-flow regime. The calibration uncertainty in basins with summer regime exceeds in many basins 60% even if the model is calibrated by the same objective function but in different calibration periods. This finding confirms and quantifies the potential impact of time stability of model parameters reported by Merz et al. (2011). The model parameters calibrated in colder periods with relatively larger runoff generation rates tend to overestimate low flows, particularly in basins with summer low-flow regime and in warmer and drier parts of the simulation period. The results indicate that the time stability of model parameters is not sensitive to the weighting of normal (M_E) and logarithmic transformed (M_E^{log}) Nash-Sutcliffe efficiency in the objective function used for calibration. The exception is the case of using only M_E with no weight on M_E^{log}, which does not allow accurate low-flow simulations. This finding partly supports the studies that propose logarithmically transformed discharge values for calibrating hydrologic models with a focus on low flows (please see review in Pushpalatha et al., 2012). Our results show that the impact of the objective function is larger for *SI* estimation in basins with summer regime in the reference period and for future projections of Q_{95} in basins with winter regime. Depending on the calibration variant, the change in seasonality can vary within more than three months, which clearly indicates a shift in the main hydrologic processes causing the low flows.

The climate change signals captured in selected scenarios are well within the range of the projections of the ENSEMBLES regional climate simulations for Europe (van der Linden and Mitchell, 2009; Heinrich and Gobiet, 2011). Jacob et al. (2015) showed that the most recent regional climate simulations over Europe, accomplished by the EURO-CORDEX initiative (RCPs, Moss et al., 2010), are rather similar to the older ENSEMBLES simulations with respect to the climate change signal and the spatial patterns of change. Although this ensemble of four scenario runs seems rather small, the selection accomplished by the reclip:century consortium was not arbitrary, but based quantitative metrics. Prein et al. (2011) investigated the performance of all GCMs in CMIP3 for Central Europe based on a performance index including various parameters. They found that for the given domain the

ECHAM5 and the HADCM3 showed highest scores, which justified the selection of these GCMs for driving the RCM. In addition, these two models show different climate sensitivity, where the warming over the course of the 21st century is lower in ECHAM5 and higher in HADCM3. This feature in combination with the utilization of three different scenarios for ECHAM5 provides broad ensemble bounds, although the climate change signal of the different scenarios for the given investigation period (2021-2050) is rather similar, particularly for temperature (cf. Table 1). The projected future decrease of Q_{95} is most pronounced in the AIT_HADCM3_A1B run, particularly in basins with summer low-flow regime in the low lands. As indicated in Heinrich and Gobiet (2011), the climate sensitivity of HADCM3 is higher than that of ECHAM5, which translates into a higher warming rate of 2.1 °C in summer (c.f. Table 1) compared to 1.2 °C in the ECHAM5 driven run. The higher evaporative demand due to the increased air temperature signal translates into the strongest change of the summer low-flow signal.

The comparison of the ranges of low-flow indices projected for different climate scenarios and simulated by different calibration settings (i.e. objective function and calibration decade) in the reference period indicates that the variability of low-flow magnitudes is larger for simulations in the reference period, while the range of seasonality is larger for future projections. Even if the variability and uncertainty of GCM and emission scenarios can be large, the results clearly indicate the importance of selecting objective functions in hydrologic model calibration for simulating low-flow projections.

In our study, we use a 3-way ANOVA approach to decompose the contribution of climate scenarios and hydrologic model settings to the total uncertainty of low-flow projections. While previous studies (e.g. Hingray and Said 2014; Lafaysse et al., 2014, Vidal et al, 2015) assessed the variance components of a temporal change from the multi-member ensemble runs in individual basins, in our study, we lumped the temporal change to one time slice (future horizon) and assessed the variance components in a spatial context of 262 basins. The spatial synthesis of the uncertainty contribution is evaluated for two groups of basins, representing to main (summer and winter) low-flow regimes in Austria. We found that the relative contribution of three variance components - climate scenarios, calibration decade and calibration objective function differs for basins with different low-flow regimes. The uncertainty from climate scenarios dominates in basins with summer low flows, however in basins with winter low flows is the relative contribution from hydrological modelling

significantly larger. This is consistent with previous studies that show a substantial uncertainty contribution of hydrological models in basins dominated by snow and ice melt (Addor et al.,2014, Vidal et al., 2015).

The assessment in Austria enabled us to account for one conceptual hydrologic model and two different low-flow regimes. In the future we plan to extend such comparative assessment to more types of low flows (e.g. as classified in Van Loon and Van Lanen, 2012), their combinations linked with changes in land use and management at the wider, European scale, as well as to account for hydrologic models of different complexity, wider range of climate scenarios and different downscaling techniques. This will allow us to shed more light on the factors controlling the possible scenarios of low-flow and water resources changes in the future.

From the practical point of view, the projections of Q_{95} changes and related uncertainties are an essential input to water quality modelling. The exceedance of environmental quality standards (BGBl II Nr. 99/2010; Zessner, 2008) in case of emissions from point sources (e.g. waste water treatment plants) increases the vulnerability of water resources, particularly during low-flow conditions. We therefore also plan to evaluate the impact of climate projection and hydrologic model uncertainties on the assessment of water quality and its changes.

Acknowledgements

We would like to thank the Austrian Climate and Energy Fund (Project B060362-CILFAD, Project Nr KR13AC6K11034-AQUASTRESS) for financial support. At the same time, we would like to thank the Hydrographical Service of Austria (HZB) and the Central Institute for Meteorology and Geodynamics (ZAMG) for providing hydrologic and climate data.

References

Addor, N., Rössler, O., Köplin, N., Huss, M., Weingartner, R., and Seibert, J.: Robust changes and sources of uncertainty in the projected hydrological regimes of Swiss catchments, Water Resour. Res., 50, 7541–7562, doi:10.1002/2014WR015549, 2014.

BGBl II Nr. 99/2010: Bundesgesetzblatt für die Republik Österreich, Qualitätszielverordnung Ökologie Oberflächengewässer – QZV Ökologie OG, Jahrgang 2010.

Bosshard, T., Carambia, M., Goergen, K., Kotlarski, S., Krahe, P., Zappa, M., and Schär, C.: Quantifying uncertainty sources in an ensemble of hydrological climate-impact projections, Water Resour. Res., 49, 1523–1536, doi:10.1029/2011WR011533, 2013.

Ceola, S., Arheimer, B., Baratti, E., Blöschl, G., Capell, R., Castellarin, A., Freer, J., Han, D., Hrachowitz, M., Hundecha, Y., Hutton, C., Lindström, G., Montanari, A., Nijzink, R., Parajka, J., Toth, E., Viglione, A., and Wagener, T.: Virtual laboratories: new opportunities for collaborative water science, Hydrol. Earth Syst. Sci., 19, 2101-2117, doi:10.5194/hess-19-2101-2015, 2015.

Coron L., Andréassian V., Perrin C., Lerat J., Vaze J., Bourqui M., and Hendrickx F.: Crash testing hydrological models in contrasted climate conditions: An experiment on 216 Australian catchments, Water Resources Research, 48 (5), doi: 10.1029/2011WR011721, 2012.

Dams, J., Nossent, J., Senbeta, T.B., Willems, P., and Batelaan, O.: Multi-model approach to assess the impact of climate change on runoff, Journal of Hydrology, 529(3),1601–1616 doi:10.1016/j.jhydrol.2015.08.023, 2015.

Dobler, C., Hagemann, S., Wilby, R. L., and Stötter, J.: Quantifying different sources of uncertainty in hydrological projections in an Alpine watershed, Hydrol. Earth Syst. Sci., 16, 4343–4360, doi:10.5194/hess-16-4343-2012, 2012.

Duan, Q., Sorooshian, S., and Gupta, V.K.: Effective and efficient global optimization for conceptual rainfall-runoff models, Water Resources Research, 28, 1015–1031, 1992.

Feyen, L., and Dankers, R.: Impact of global warming on streamflow drought in Europe, J. Geophys. Res., 114, D17116, doi:10.1029/2008JD011438, 2009.

Finger, D., Heinrich, G., Gobiet, A., and Bauder, A.: Projections of future water resources and their uncertainty in a glacierized catchment in the Swiss Alps and the subsequent effects on

hydropower production during the 21st century, Water Resour. Res., 48, W02521, doi:10.1029/2011WR010733, 2012.

Fleig, A.K., Tallaksen, L.M., Hisdal, H., and Demuth, S.: A global evaluation of streamflow drought characteristics, Hydrol. Earth Syst. Sci., 10, 535–552, 2006.

Forzieri, G., Feyen, L., Rojas, R., Flörke, M., Wimmer, F., and Bianchi, A.: Ensemble projections of future streamflow droughts in Europe, Hydrol. Earth Syst. Sci., 18, 85–108, doi: 10.5194/hess-18-85-2014, 2014.

Gaál, L., Szolgay, J., Kohnová, S., Parajka, J., Merz, R., Viglione, A., and Blöschl, G.: Flood timescales: Understanding the interplay of climate and catchment processes through comparative hydrology, Water Resources Research, 48(4), W04511, doi: 10.1029/2011WR011509, 2012.

Hingray, B., and Said, M.: Partitioning internal variability and model uncertainty components in a multimember multimodel ensemble of climate projections, Journal of Climate, 27, 17, 6779, doi: http://dx.doi.org/10.1175/JCLI-D-13-00629.1, 2014.

Huang, S., Krysanova, V., and Hattermann, F. F.: Projection of low flow conditions in Germany under climate change by combining three RCMs and a regional hydrological model, Acta Geophysica, 61 (1), 151-193, 2013.

Chauveau, M., Chazot, S., Perrin, C., Bourgin, P., Sauquet, E., Vidal, J., Rouchy, N., Martin, E., David, J., Norotte, T., Maugis, P., and de Lacaze, X.: What impacts of climate change on surface hydrology in France by 2070?, La Houille Blanche, (4), 5-15, 2013.

Chiew, F. H. S., Zheng, H., and Vaze, J.: Implication of calibration period on modelling climate change impact on future runoff, Proc. IAHS, 371, 3-6, doi:10.5194/piahs-371-3-2015, 2015.

Heinrich, G. and Gobiet, A.: reclip:century 1 Research for Climate Protection: Century Climate Simulations: Expected Climate Change and its Uncertainty in the Alpine Region, ACRP final report reclip:century part D, Graz, Austria, 48 pp, 2011.

Jacob, D., Petersen, J., Eggert, B., Alias, A., Christensen, O. B., Bouwer, L., Braun, A., Colette, A., Déqué, M., Georgievski, G., Georgopoulou, E., Gobiet, A., Menut, L., Nikulin, G., Haensler, A., Hempelmann, N., Jones, C., Keuler, K., Kovats, S., Kröner, N., Kotlarski, S., Kriegsmann, A., Martin, E., Meijgaard, E., Moseley, C., Pfeifer, S., Preuschmann, S., Radermacher, C., Radtke, K., Rechid, D., Rounsevell, M., Samuelsson, P., Somot, S.,

Soussana, J.-F., Teichmann, C., Valentini, R., Vautard, R., Weber, B. and Yiou, P.: EURO-CORDEX: new high-resolution climate change projections for European impact research Regional Environmental Change, Springer, Berlin, Heidelberg, Germany, 1-16, 2013.

Koffler, D., and Laaha, G.: lfstat: Calculation of Low Flow Statistics for daily stream flow data. R package version 0.5. http://CRAN.R-project.org/package=lfstat, (last access: 20 November 2015), 2014.

Laaha, G., and Blöschl, G.: Seasonality indices for regionalizing low flows, Hydrolog. Process., 20, 3851–3878, doi: 10.1002/hyp.6161, 2006.

Laaha, G. and Blöschl, G.: A national low flow estimation procedure for Austria, Hydrological Sciences Journal, 52(4), 625–644, 2007.

Laaha, G., Parajka, J., Viglione, A., Koffler, D., Haslinger, K., Schöner, W., Zehetgruber, J., and Blöschl, G.: A three-pillar approach to assess climate impacts on low flows, submitted to HESSD, 2015.

Lafaysse, M., Hingray, B., Mezghani, A., Gailhard, J., and Terray, L.: Internal variability and model uncertainty components in future hydrometeorological projections: The Alpine Durance basin, Water Resour. Res., 50, 3317–3341, doi:10.1002/ 2013WR014897, 2014.

Loibl, W., Formayer, H., Schöner, W., Truhetz, H., Anders, I., Gobiet, A., Heinrich, G., Köstl, M., Nadeem, I., Peters Anders, J., Schicker, I., Suklitsch, M., and Züger, H.: reclip:century 1 Research for Climate Protection: Century Climate Simulations: Models, Data and GHG Scenarios, Simulations, ACRP final report reclip:century part A, Vienna, 22 pp, 2011.

Merz, R., Parajka, J., and Blöschl, G.: Time stability of catchment model parameters: Implications for climate impact analyses, Water Resour. Res., 47, W02531, doi:10.1029/2010WR009505, 2011.

Moss, R. H., Edmonds, J. A., Hibbard, K. A., Manning, M. R., Rose, S. K., van Vuuren, D. P., Carter, T. R., Emori, S., Kainuma, M., Kram, T., Meehl, G. A., Mitchell, J. F. B., Nakicenovic, N., Riahi, K., Smith, S. J., Stouffer, R. J., Thomson, A. M., Weyant, J. P., and Wilbanks, T. J.: The next generation of scenarios for climate change research and assessment, Nature, 463, 747-756, 2010.

Najafi, M.R., Moradkhani, H., and Jung, I.W.: Assessing the uncertainties of hydrologic model selection in climate change impact studies, Hydrol. Process. 25, 2814–2826, DOI: 10.1002/hyp.8043, 2011.

Nakicenovic, N., Alcamo, J., Davis, G., de Vries, B., Fenhann, J., Gaffin, S., Gregory, K., Grübler, A., Jung, T. Y., Kram, T., La Rovere, E. L., Michaelis, L., Mori, S., Morita, T., Pepper, W., Pitcher, H., Price, L., Raihi, K., Roehrl, A., Rogner, H.-H., Sankovski, A., Schlesinger, M., Shukla, P., Smith, S., Swart, R., van Rooijen, S., Victor, N. and Dadi, Z.: IPCC Special Report on Emissions Scenarios. Cambridge University Press: Cambridge, United Kingdom and New York, 599 pp, 2000.

Parajka, J., Merz, R., and Blöschl, G.: Uncertainty and multiple objective calibration in regional water balance modelling: case study in 320 Austrian catchments, Hydrol. Process., 21, 435–446, doi:10.1002/hyp.6253, 2007.

Parajka, J., and Blöschl, G.: The value of MODIS snow cover data in validating and calibrating conceptual hydrologic models, Journal of Hydrology, 358, 240–258, 2008.

Prein, A. F., Gobiet, A. and Truhetz, H.: Analysis of uncertainty in large scale climate change projections over Europe, Met. Zet., 20 (4), 383-395, 2011.

Prudhomme, Ch., and Davies, H.: Assessing uncertainties in climate change impact analyses on the river flow regimes in the UK. Part 2: future climate, Climatic Change, 93, 177–195, DOI 10.1007/s10584-008-9464-3, 2009.

Skoien, J.O., Blöschl, G., Laaha, G., Pebesma, E., Parajka, J., and Viglione, A.: rtop: An R package for interpolation of data with a variable spatial support, with an example from river networks, Computers & Geosciences, Volume 67, Pages 180-190, http://dx.doi.org/10.1016/j.cageo.2014.02.009, 2014.

Van der Linden, P., and Mitchell, J. F. B. (eds.): ENSEMBLES: Climate Change and its Impacts: Summary of research and results from the ENSEMBLES project, Met Office Hadley Centre, Exeter, United Kingdom, 160pp, 2009.

Van Loon, A. F. and Van Lanen, H. A. J.: A process-based typology of hydrological drought, Hydrol. Earth Syst. Sci., 16, 1915–1946, doi:10.5194/hess-16-1915-2012, 2012.

Van Loon, A.F., Ploum, S.W., Parajka, J., Fleig, A.K., Garnier, E., Laaha, G., and Van Lanen, H.A.J.: Hydrological drought types in cold climates: quantitative analysis of causing factors and qualitative survey of impacts, Hydrol. Earth Syst. Sci., 19, 1993–2016, 2015.

Vidal, J.-P., Hingray, B., Magand, C., Sauquet, E., and Ducharne, A.: Hierarchy of climate and hydrological uncertainties in transient low flow projections, Hydrol. Earth Syst. Sci. Discuss., 12, 12649-12701, doi:10.5194/hessd-12-12649-2015, 2015.

Viglione, A., Parajka, J., Rogger, M., Salinas, J.L., Laaha, G., Sivapalan, M., and Blöschl, G.: Comparative assessment of predictions in ungauged basins; Part 3: Runoff signatures in Austria. Hydrology and Earth System Sciences, 17, 2263-2279, 2013.

Viglione, A., and Parajka, J.: TUWmodel: Lumped Hydrological Model for Education Purposes. R package version 0.1-4. http://CRAN.R-project.org/package=TUWmodel, (last access: 20 November 2015), 2014.

von Storch, H., and Zwiers, F.W.: Statistical analysis in climate research, Cambridge University press, ISBN 0 521 45071 3, 484pp, 1999.

Zessner M.: Transboundary pollution and water quality policies in Austria, Water Science & Technology, 58.10, 2008.

Table 1. TUWmodel parameters. Calibration range is given for parameters calibrated by an automatic routine. Parameters with fixed value are not calibrated.

Model parameter	Definition	Model component	Calibration range
SCF	Snow correction factor (dimensionless)	Snow	1.0-1.5
DDF	Degree-day factor (mm/°C day)	Snow	0.0-5.0
T_R	Threshold temperature for rain (°C)	Snow	2.0
T_S	Threshold temperature for snow (°C)	Snow	0.0
T_M	Melt temperature (°C)	Snow	-1.0-3.0
LP/FC	Ratio of limit for potential evapotranspiration and FC (dimensionless)	Soil	0.0-1.0
FC	Maximum soil moisture storage (mm)	Soil	0.0-600.0
BETA	Nonlinearity parameter of runoff generation (dimensionless)	Soil	0.0-20.0
K_0	Storage coefficient of additional outlet (days)	Runoff	0.0-2.0
K_1	Fast storage coefficient (days)	Runoff	2.0-30.0
K_2	Slow storage coefficient (days)	Runoff	30.0-250.
C_P	Percolation rate (mm/d)	Runoff	0.0-8.0
C_R	Free routing coefficient ($days^2$/mm)	Runoff	25.0
LS_{UZ}	Storage capacity threshold (mm)	Runoff	1.0-100.0
Bmax	Routing parameter (days)	Runoff	10.0

Table 2. Summary of seasonal and annual changes in the mean basin precipitation and air temperature as simulated by four selected RCM runs. The first value and values in the brackets are the median and range (min/max) of differences between the future (2021-2050) and reference (1978-2007) periods in 262 basins. Winter and summer seasons are defined as December-May and June-November, respectively.

Delta change	WEGC* ECHAM5 A1B	ZAMG** ECHAM5 A2	AIT*** HADCM3 A1B	ZAMG ECHAM5 B1
Air temperature winter (°C)	+1.5 (0.9/1.7)	+0.7 (-1.1/2.1)	+1.3 (0.8/1.5)	+1.0 (-0.8/2.5)
Air temperature summer (°C)	+1.2 (0.8/1.7)	+0.9 (-0.1/2.2)	+2.1 (1.4/2.4)	+1.3 (0.4/2.5)
Air temperature year (°C)	+1.3 (0.9/1.5)	+0.8 (-0.4/2.2)	+1.7 (1.2/1.9)	+1.2 (0.0/2.5)
Precipitation winter (%)	+8.2 (-0.7/16.2)	-1.5 (-5.8/6.4)	+1.3 (-9.6/6.8)	0.0 (-8.5/3.3)
Precipitation summer (%)	-6.2 (-9.9/3.7)	+0.2 (-8.9/5.7)	-5.0 (-13.5/0.2)	-2.3 (-6.3/2.5)
Precipitation year (%)	+0.9 (-4.6/8.7)	-0.9 (-4.1/3.4)	-2.0 (-9.3/1.8)	-1.2 (-5.5/2.8)

*WEGC= Wegener Center for Climate and Global Change

**ZAMG= Zentralanstalt für Meteorologie und Geodynamik

***AIT= Austrian Institute of Technology

Figure captions:

Figure 1. Topography of Austria and location of 262 river flow gauges. Colour and symbol size of the gauges represent seasonality of low flows *SI* and its strength (*r*) in the period 1976-2008, respectively. The SI and its strength are estimated by R lfstat package (Koffler and Laaha, 2014).

Figure 2. Mean annual air temperature (MAT, top), precipitation (MAP, middle) and runoff (MAR, bottom) for basins with summer (yellow/red) and winter (blue) low-flow minima (Fig.1). Thin lines represent the median of mean annual values of MAT, MAP and MAR. Thick lines indicate the average for each of the three periods: 1976-86, 1987-97 and 1998-08. Scatter (i.e. 75% and 25%- percentiles) indicates the variability between the basins.

Figure 3. Runoff model efficiency (Z_Q) for different calibration weights w_Q in three different calibration periods. Lines represent the medians, scatter (i.e. 75%-25% percentiles) shows the Z_Q variability over basins with dominant winter (blue) and summer (orange) low-flow regime.

Figure 4. Difference between simulated and observed low-flow characteristics (top panels low-flow quantile Q_{95}, bottom panels seasonality index *SI*) for different calibration variants (w_Q) and calibration periods. Lines represent the median, scatter (i.e. 75%-25% percentiles) show the variability over basins with dominant winter (blue) and summer (orange) low flow regime. The differences are estimated between model simulations and observations in the entire reference period 1976-2008.

Figure 5. Comparison of observed (blue) and simulated (red) flow for Hoheneich/Braunaubach, 291.5 km^2). Thick lines show flows below low-flow quantile Q_{95}. Model simulations are based on calibration variant w_Q=0.5 in the period 1998-2008. The relative difference between Q_{95} estimated from simulated and observed flows is 8%.

Figure 6. Uncertainty of Q_{95} model simulations estimated from 11 calibration variants calibrated in the same calibration period (right panels, top - calibration period 1976-1986, bottom - calibration period 1998-2008) and from three calibration periods calibrated by the same calibration variant (left panels, top w_Q=0.5, bottom w_Q=0.0). The uncertainty is expressed as the range of relative differences (%) between simulated and observed Q_{95} obtained by particular calibration variants in the period 1976-2008. Colour patterns in the background show the interpolated ranges by using top-kriging method (Skoien et al., 2014).

Figure 7. Uncertainty of simulations of low-flow seasonality (*SI*) estimated from 11 calibration variants calibrated in the same calibration period (right panels, top - calibration period 1976-1986, bottom - calibration period 1998-2008) and from three calibration periods calibrated by the same calibration variant (left panels, top w_Q=0.5, bottom w_Q=0.0). The uncertainty is expressed as the range of differences (days) between simulated and observed *SI* in the period 1976-2008. Colour patterns in the background show the interpolated ranges by using top-kriging.

Figure 8. Projections of low flows for selected climate scenarios and calibration variants. Line represents the medians, scatter (i.e. 75%-25% percentiles) shows the variability over 262 basins. Top and bottom panels show projected changes of low-flow quantiles Q_{95} and seasonality index *SI* in basins with winter (blue) and summer (orange) low-flow regimes, respectively. Projections indicate future changes with respect to the reference period 1976-2008. Calibration variants are calibrated in the period 1998-2008.

Figure 9. Projections of low-flow quantiles Q_{95} changes for four climate scenarios in 262 Austrian basins. Model simulations are based on variant w_Q=0.5 calibrated in the period 1998-2008. Colour patterns in the background show the interpolated projections by using top-kriging.

Figure 10. Projections of changes in low-flow seasonality (*SI*) for four climate scenarios in 262 Austrian basins. Model simulations are based on variant w_Q=0.5 calibrated in the period 1998-2008. Colour patterns in the background show the interpolated projections by using top-kriging.

Figure 11. Uncertainty of Q_{95} model projections of low flows for four different climate scenarios. The uncertainty is expressed as the range of relative differences (%) between Q_{95} simulated in the future and reference period obtained for 11 calibration variants calibrated in three calibration periods. Colour patterns in the background show the interpolated ranges by using top-kriging.

Figure 12. Uncertainty of model projections of low-flow seasonality for four different climate scenarios. The uncertainty is expressed as the range of relative differences (%) between seasonality occurrence (*SI*) simulated in the future and reference period obtained for 11 calibration variants calibrated in three calibration periods. Colour patterns in the background show the interpolated ranges by using top-kriging.

Figure 13. Total uncertainty of model projections of low flows for four different climate scenarios, 11 calibration variants and three calibration periods. The uncertainty is expressed as the range of Q_{95} (left panel) and seasonality (right panel) of differences between model simulations in the future and reference periods. Bottom panels show the ratio between the range of climate projections to the range of differences in the reference period. Colour patterns in the background show the interpolated ranges by using top-kriging.

Figure 14. Relationship between the uncertainty ratio between calibration and projection uncertainty and basin area (left panels), mean basin elevation (middle panels) and aridity index (right panels). Top and bottom panels show the uncertainty ratio for the low-flow quantile (Q95) and seasonality index (*SI*), respectively. Basins with winter low-flow seasonality are plotted in blue, basins with summer low-flow seasonality are in yellow.

Figure 15. Relative contribution of the three variance components (i.e. climate scenario, calibration decade and objective function) to the overall uncertainty of future low flow projection in basins with winter (left panel) and summer (right panel) low-flow regime. The boxes and whiskers show 25%- and 75%- percentiles and 5%- and 95%- percentiles of the uncertainty contributions in 130 (summer low-flow regime) and 132 (winter low-flow regime) basins, respectively.

1 Figures:

2

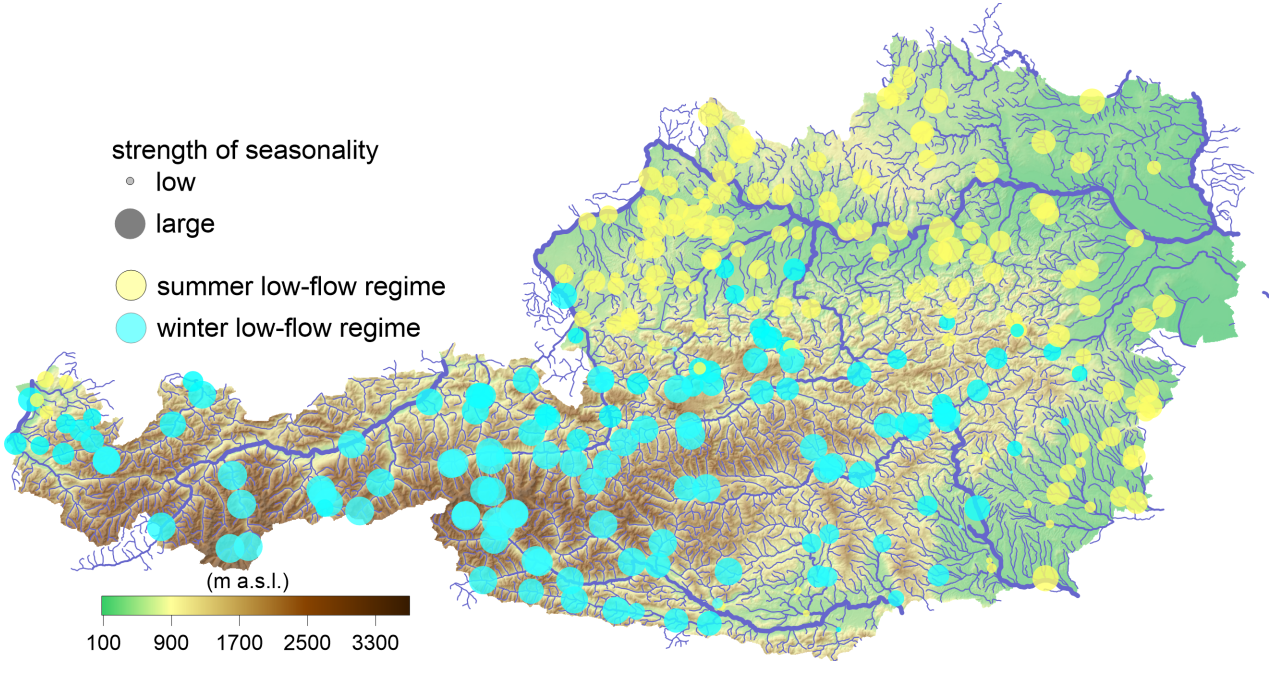
strength of seasonality
low
large
summer low-flow regime
winter low-flow regime
(m a.s.l.)
100
900
1700
2500
3300

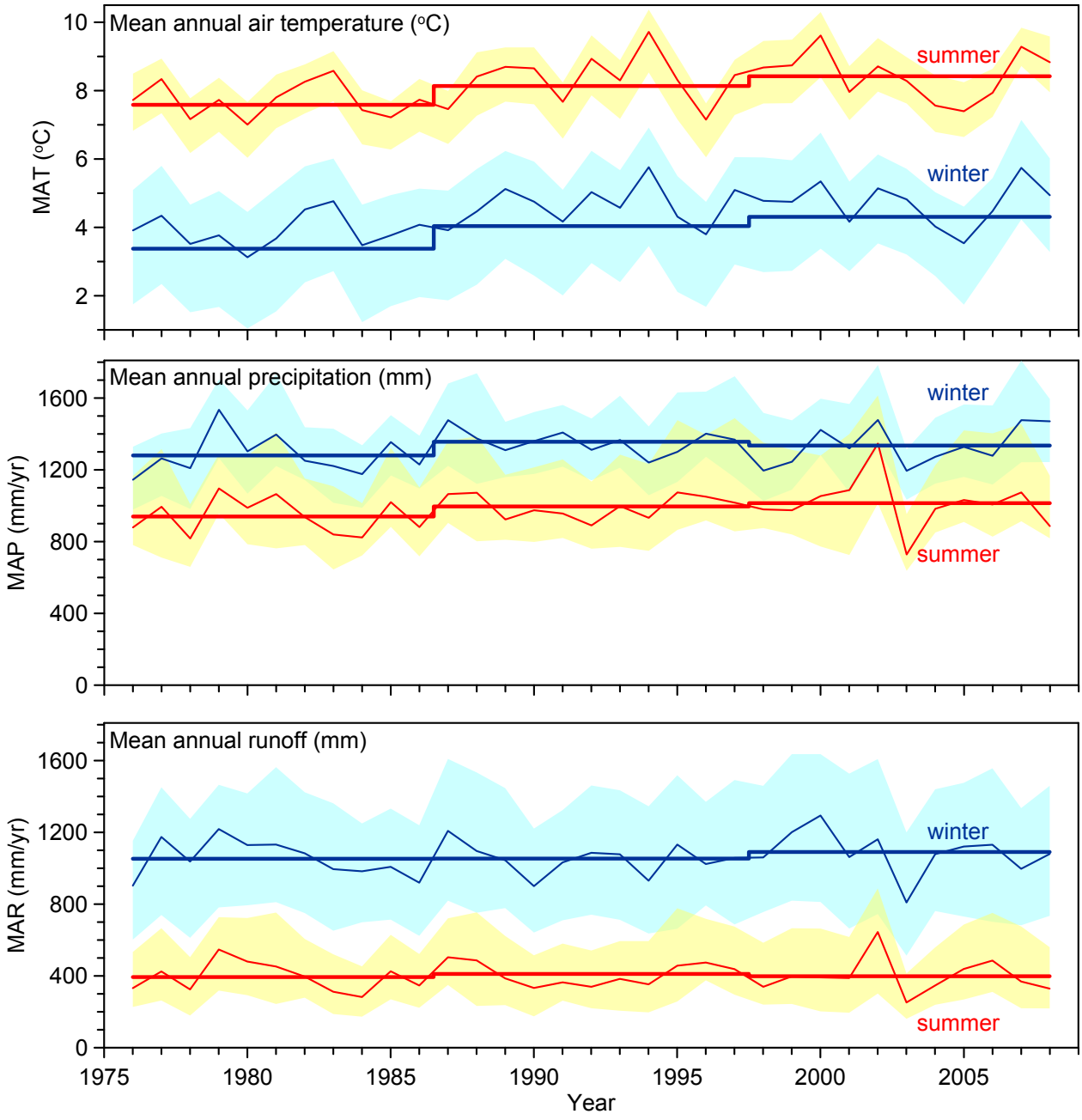
Mean annual air temperature (°C)
MAT (°C)
summer
winter
Mean annual precipitation (mm)
MAP (mm/yr)
winter
summer
Mean annual runoff (mm)
MAR (mm/yr)
winter
summer
Year

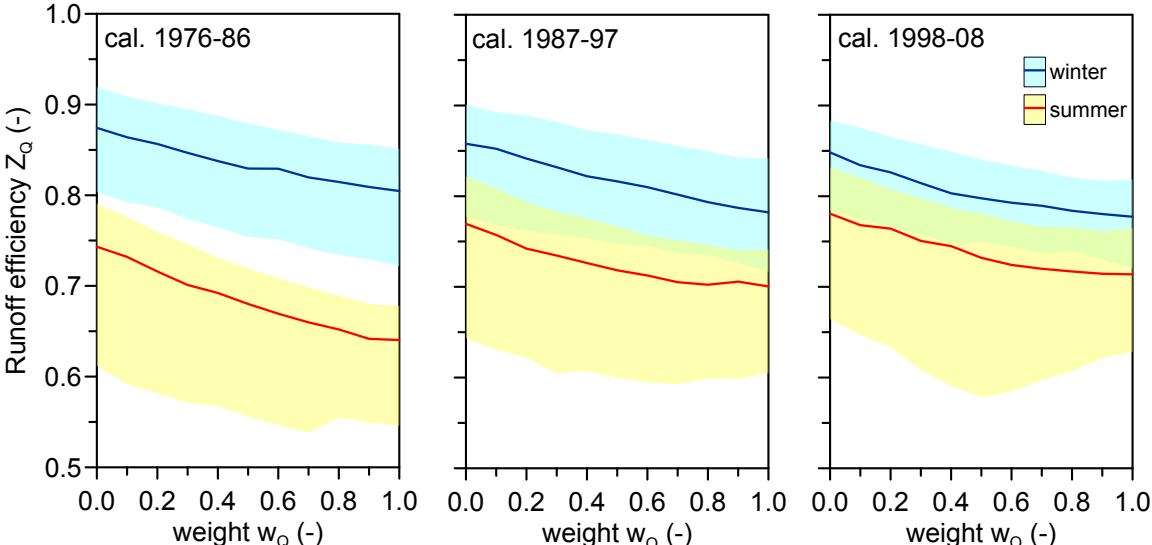
cal. 1976-86
cal. 1987-97
cal. 1998-08
winter
summer
Runoff efficiency Z_Q (-)
1.0
0.9
0.8
0.7
0.6
0.5
0.0
0.2
0.4
0.6
0.8
1.0
weight w_Q (-)

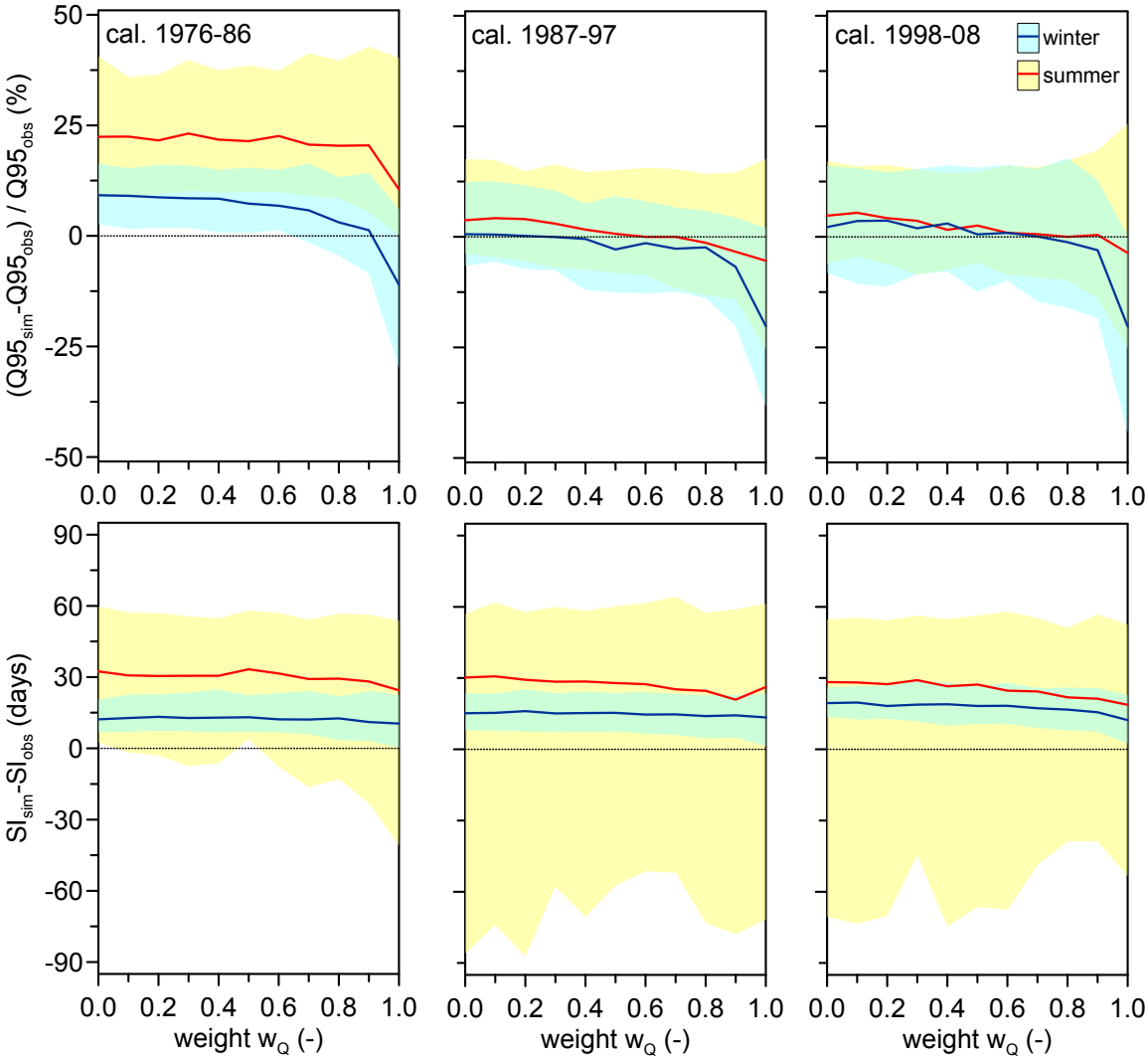
cal. 1976-86
cal. 1987-97
cal. 1998-08
winter
summer
(Q95sim-Q95obs) / Q95obs (%)
SIsim-SIobs (days)
weight wQ (-)
50
25
0
-25
-50
90
60
30
0
-30
-60
-90
0.0
0.2
0.4
0.6
0.8
1.0

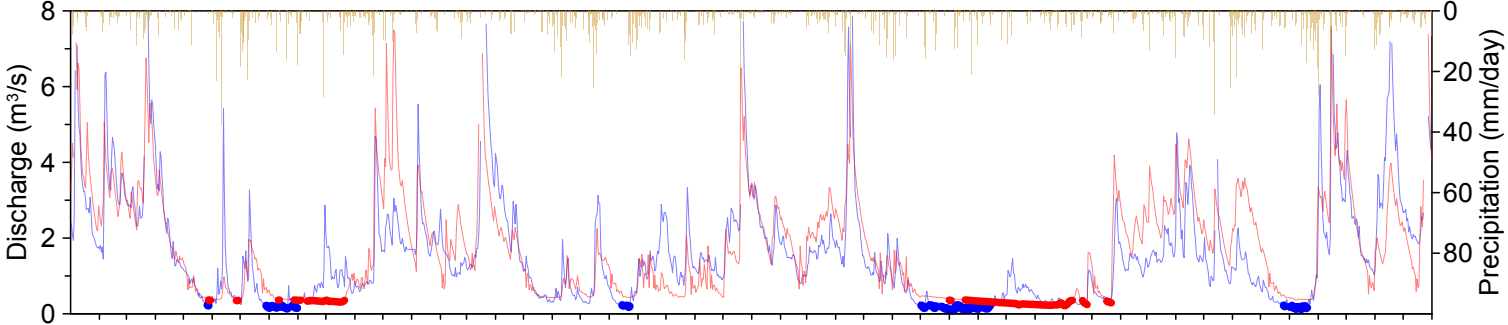
Discharge (m3/s)
Precipitation (mm/day)
0
2
4
6
8
0
20
40
60
80
1992
1993
1994
1995

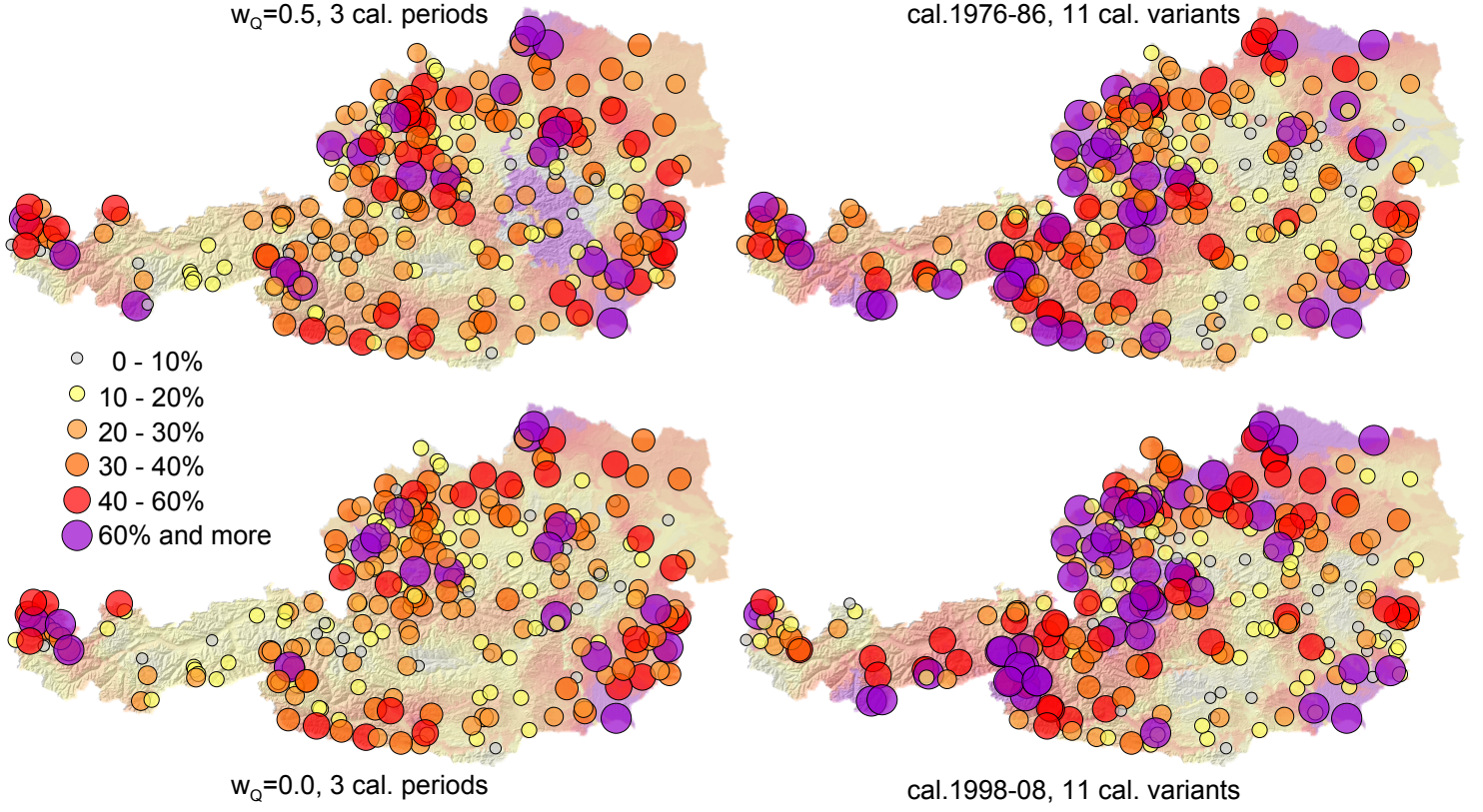
w_Q=0.5, 3 cal. periods
cal.1976-86, 11 cal. variants
0 - 10%
10 - 20%
20 - 30%
30 - 40%
40 - 60%
60% and more
w_Q=0.0, 3 cal. periods
cal.1998-08, 11 cal. variants

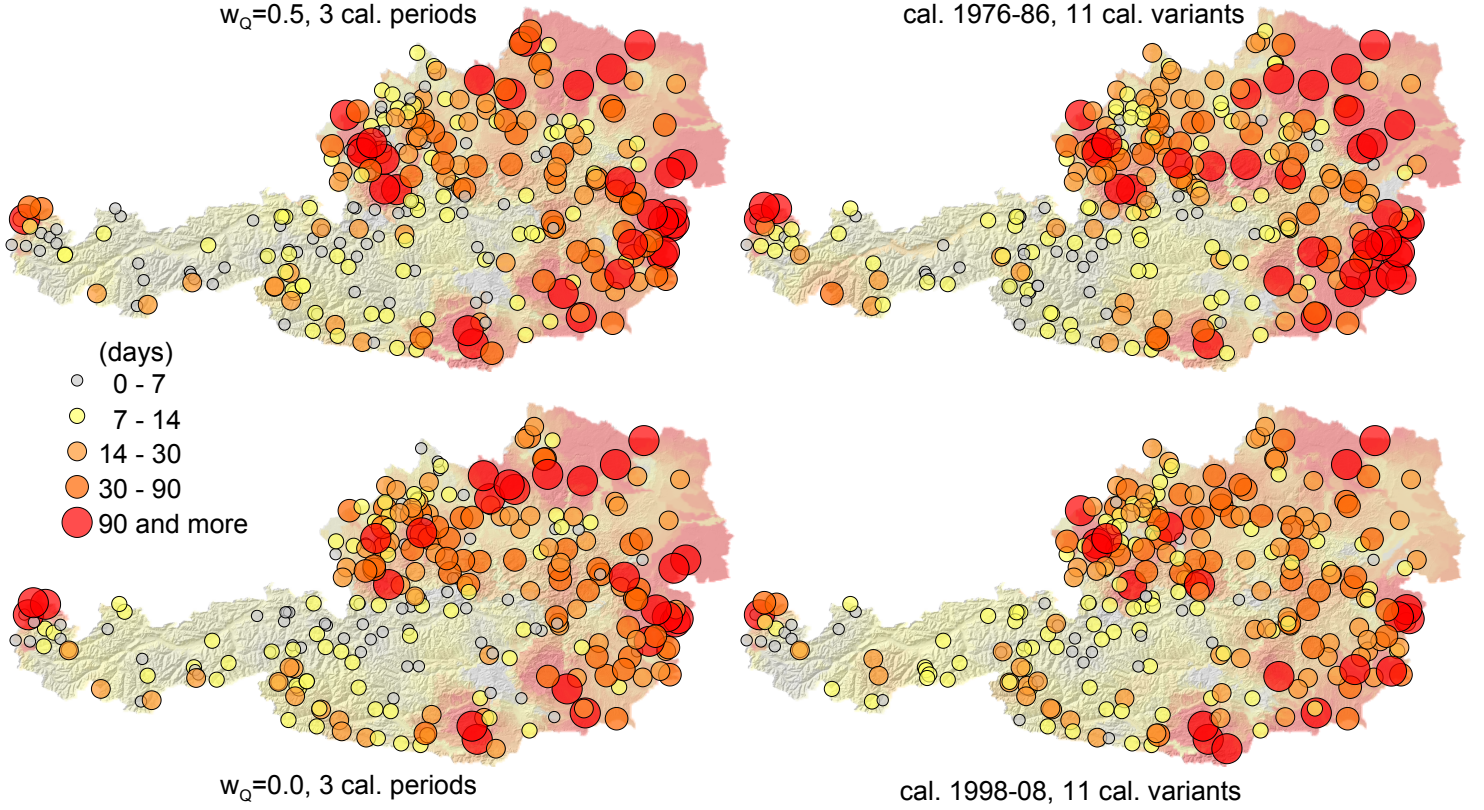
w_Q=0.5, 3 cal. periods
cal. 1976-86, 11 cal. variants
(days)
0 - 7
7 - 14
14 - 30
30 - 90
90 and more
w_Q=0.0, 3 cal. periods
cal. 1998-08, 11 cal. variants

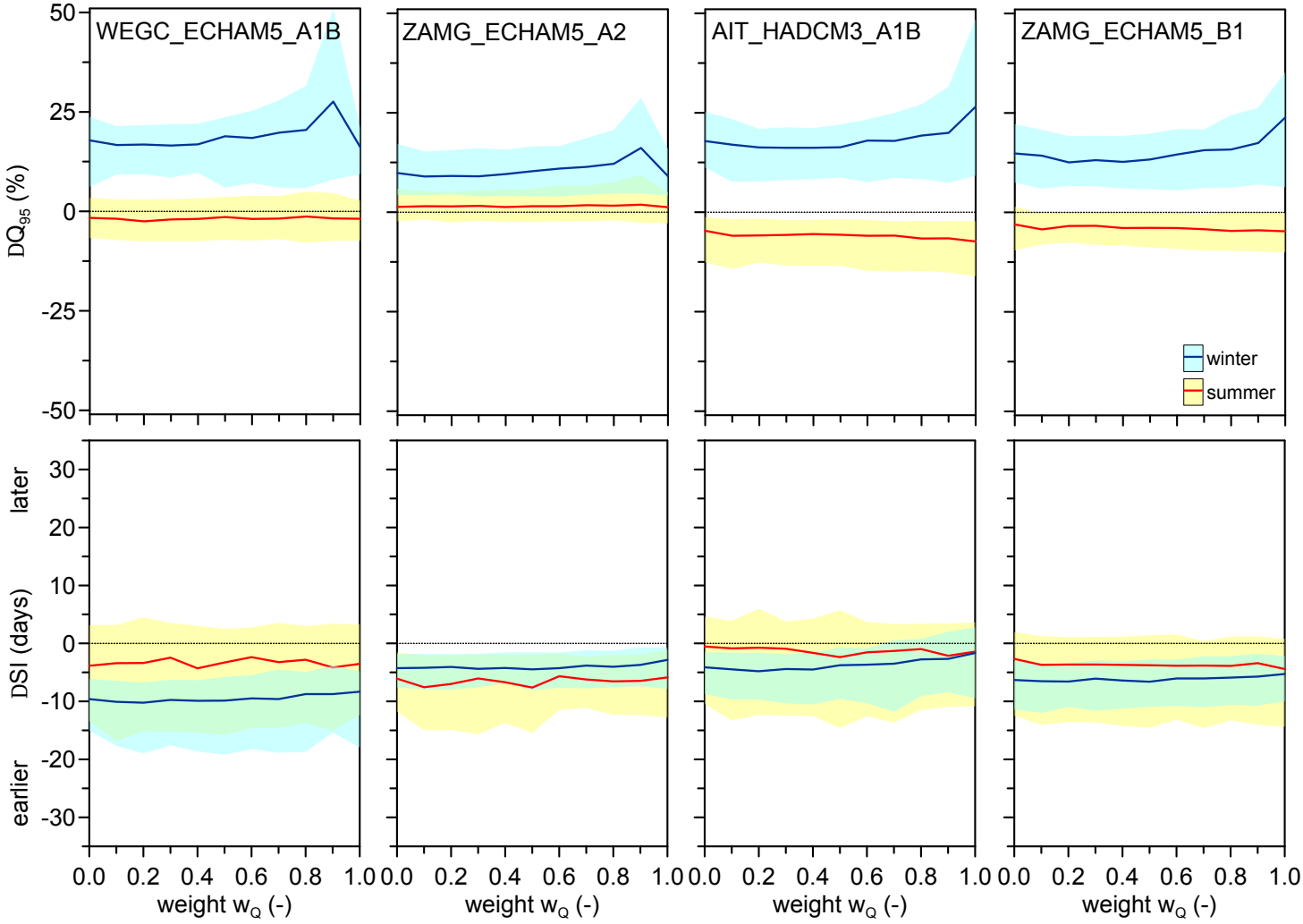
WEGC_ECHAM5_A1B
ZAMG_ECHAM5_A2
AIT_HADCM3_A1B
ZAMG_ECHAM5_B1
DQ95 (%)
50
25
0
-25
-50
winter
summer
DSI (days)
later
earlier
30
20
10
0
-10
-20
-30
0.0
0.2
0.4
0.6
0.8
1.0
weight wQ (-)

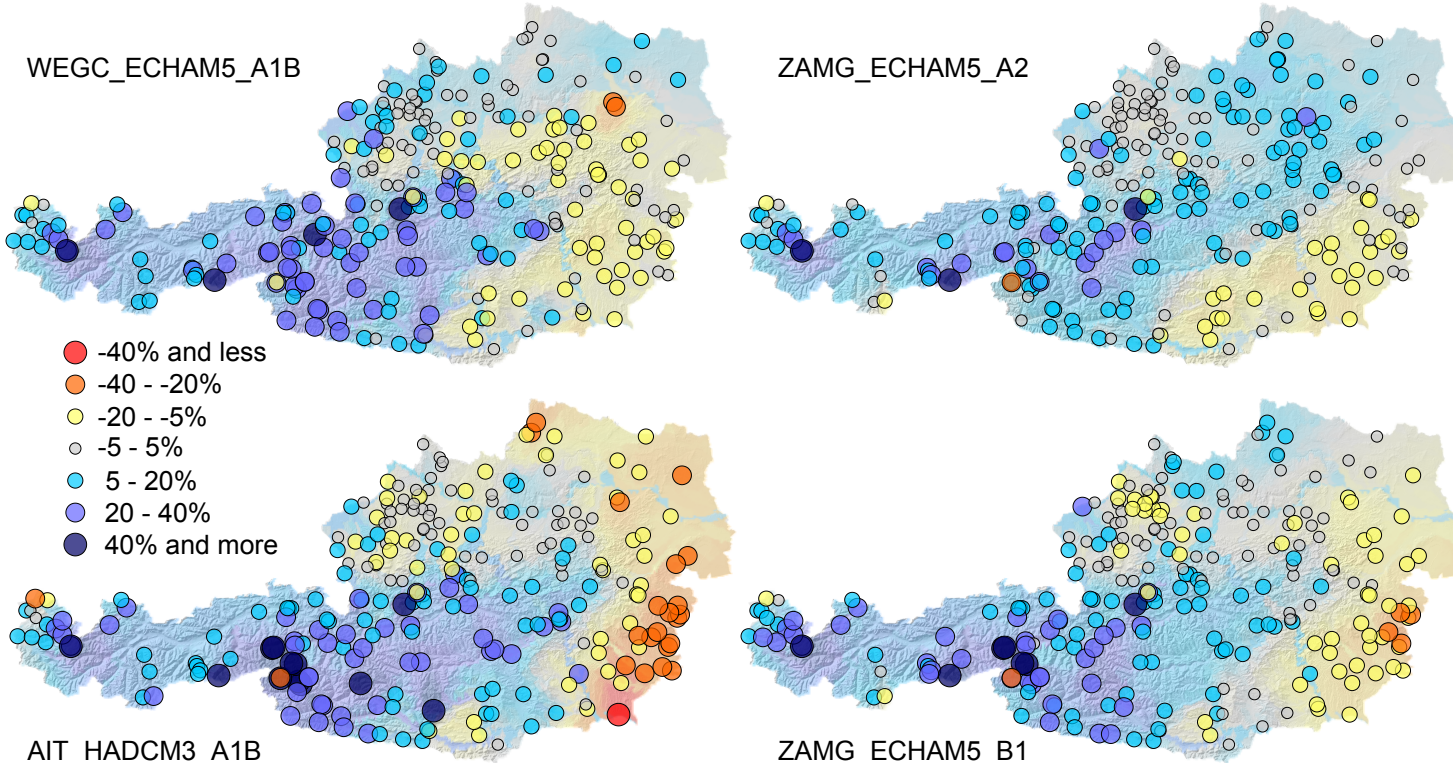
WEGC_ECHAM5_A1B
ZAMG_ECHAM5_A2
-40% and less
-40 - -20%
-20 - -5%
-5 - 5%
5 - 20%
20 - 40%
40% and more
AIT_HADCM3_A1B
ZAMG_ECHAM5_B1

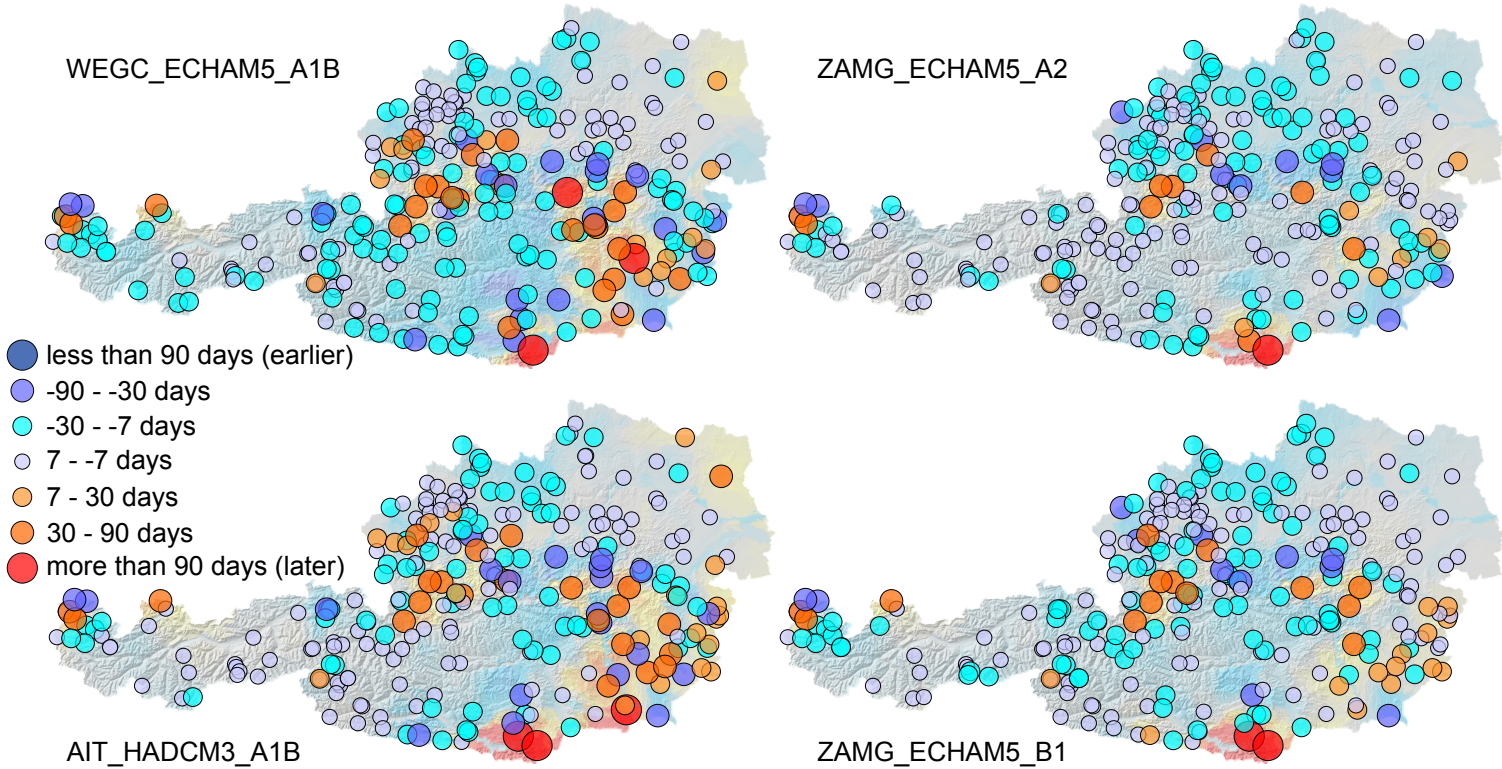
WEGC_ECHAM5_A1B
ZAMG_ECHAM5_A2
less than 90 days (earlier)
-90 - -30 days
-30 - -7 days
7 - -7 days
7 - 30 days
30 - 90 days
more than 90 days (later)
AIT_HADCM3_A1B
ZAMG_ECHAM5_B1

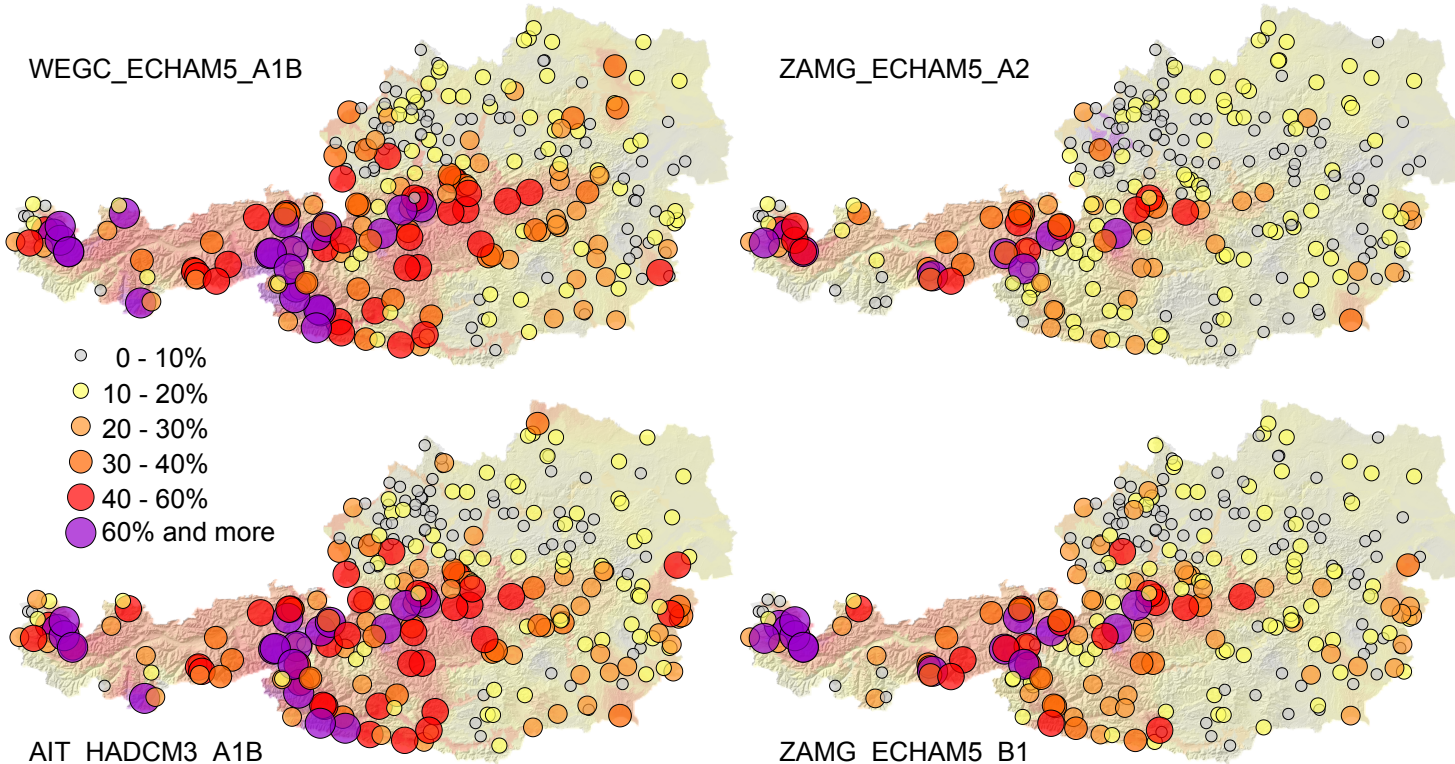
WEGC_ECHAM5_A1B
ZAMG_ECHAM5_A2
0 - 10%
10 - 20%
20 - 30%
30 - 40%
40 - 60%
60% and more
AIT_HADCM3_A1B
ZAMG_ECHAM5_B1

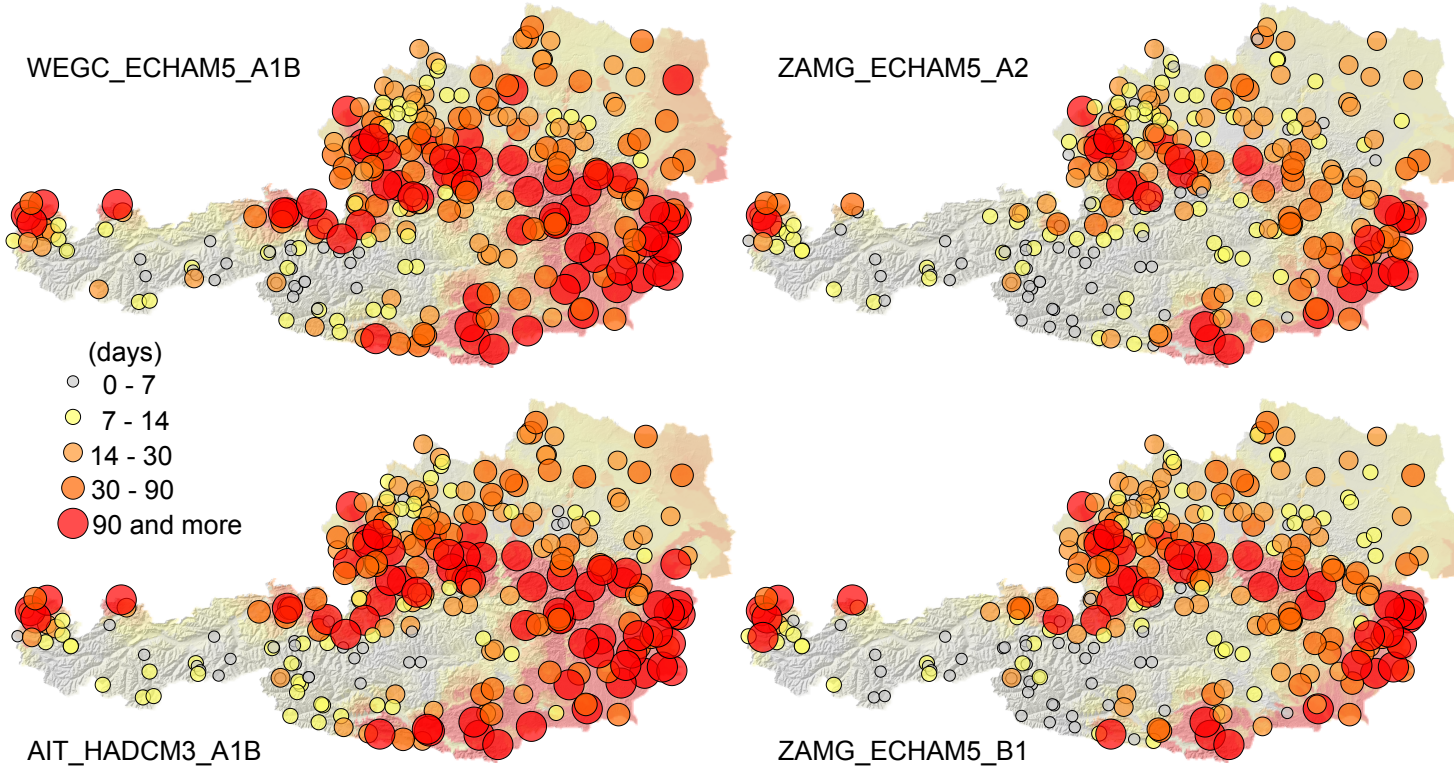
WEGC_ECHAM5_A1B
ZAMG_ECHAM5_A2
(days)
0 - 7
7 - 14
14 - 30
30 - 90
90 and more
AIT_HADCM3_A1B
ZAMG_ECHAM5_B1

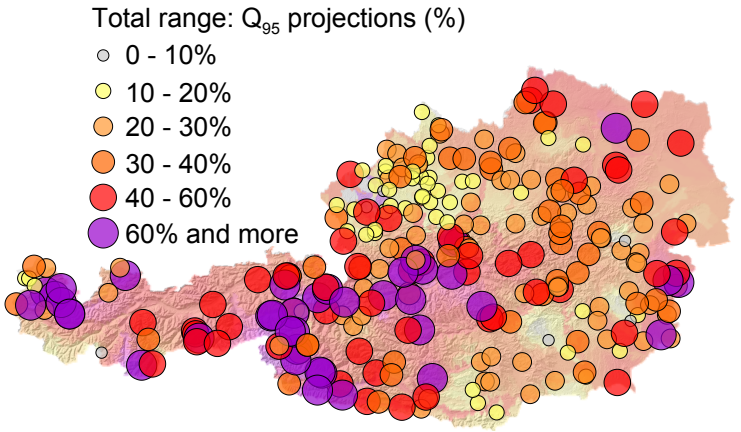
Total range: Q_{95} projections (%)
0 - 10%
10 - 20%
20 - 30%
30 - 40%
40 - 60%
60% and more

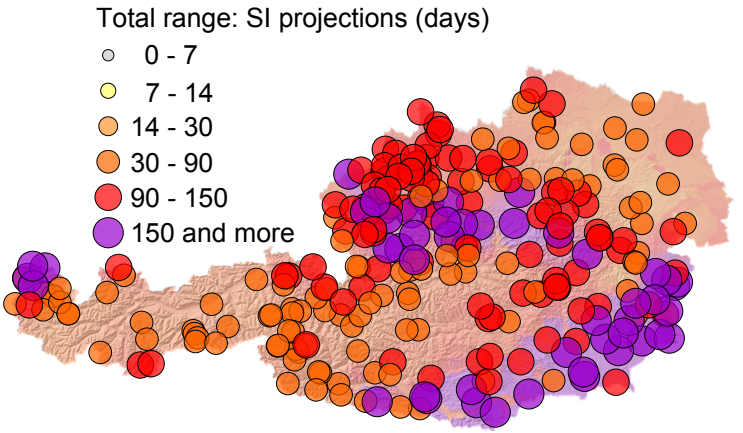
Total range: SI projections (days)
0 - 7
7 - 14
14 - 30
30 - 90
90 - 150
150 and more

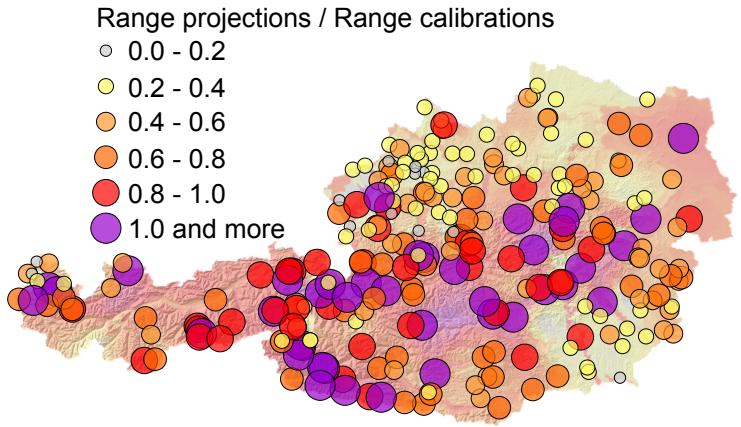
Range projections / Range calibrations
0.0 - 0.2
0.2 - 0.4
0.4 - 0.6
0.6 - 0.8
0.8 - 1.0
1.0 and more

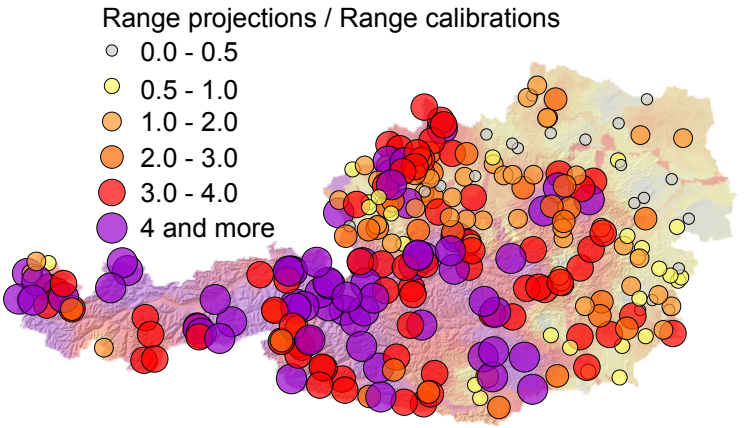
Range projections / Range calibrations
0.0 - 0.5
0.5 - 1.0
1.0 - 2.0
2.0 - 3.0
3.0 - 4.0
4 and more

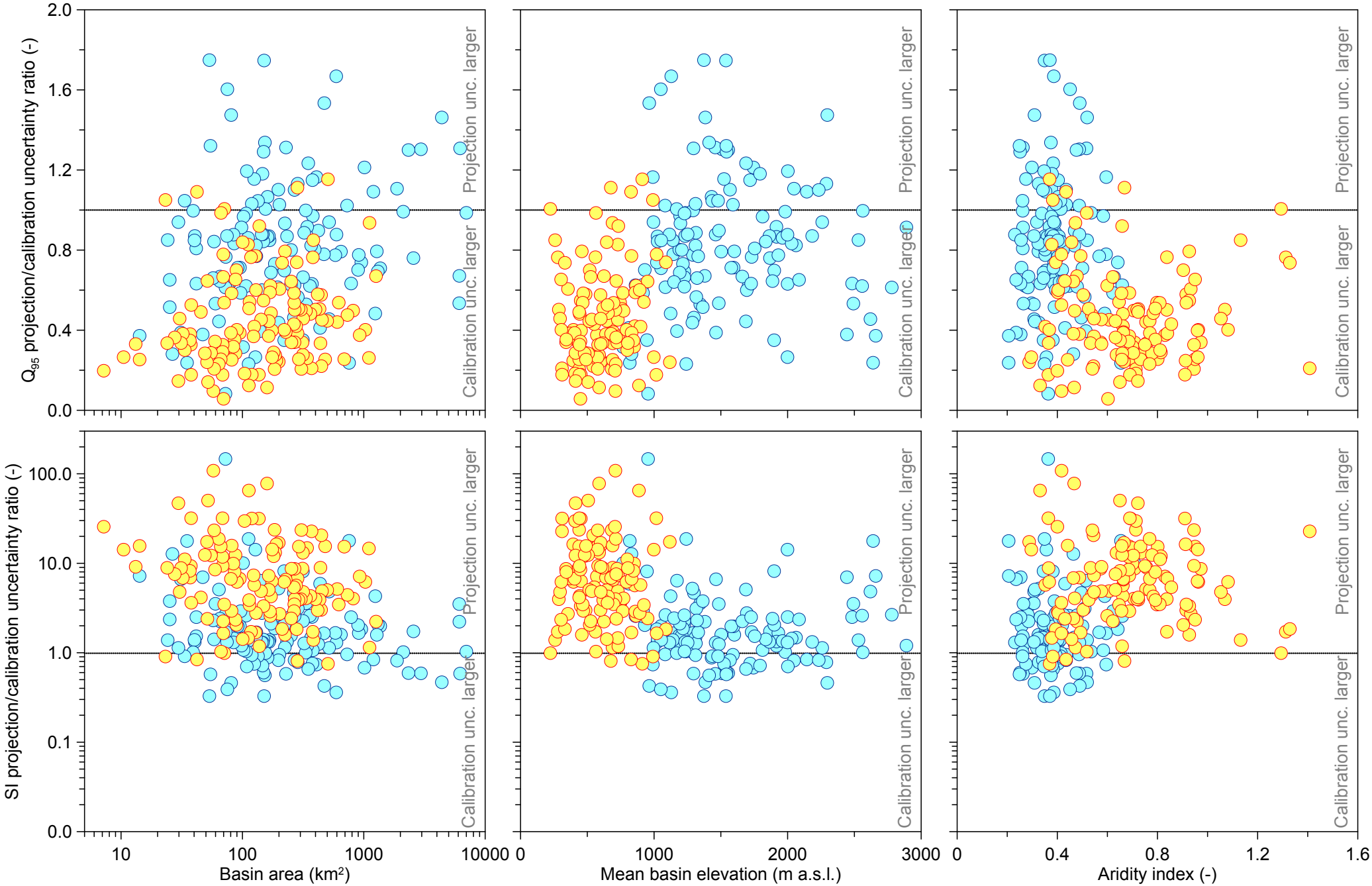
Q_{95} projection/calibration uncertainty ratio (-)
SI projection/calibration uncertainty ratio (-)
Projection unc. larger
Calibration unc. larger
Basin area (km²)
Mean basin elevation (m a.s.l.)
Aridity index (-)

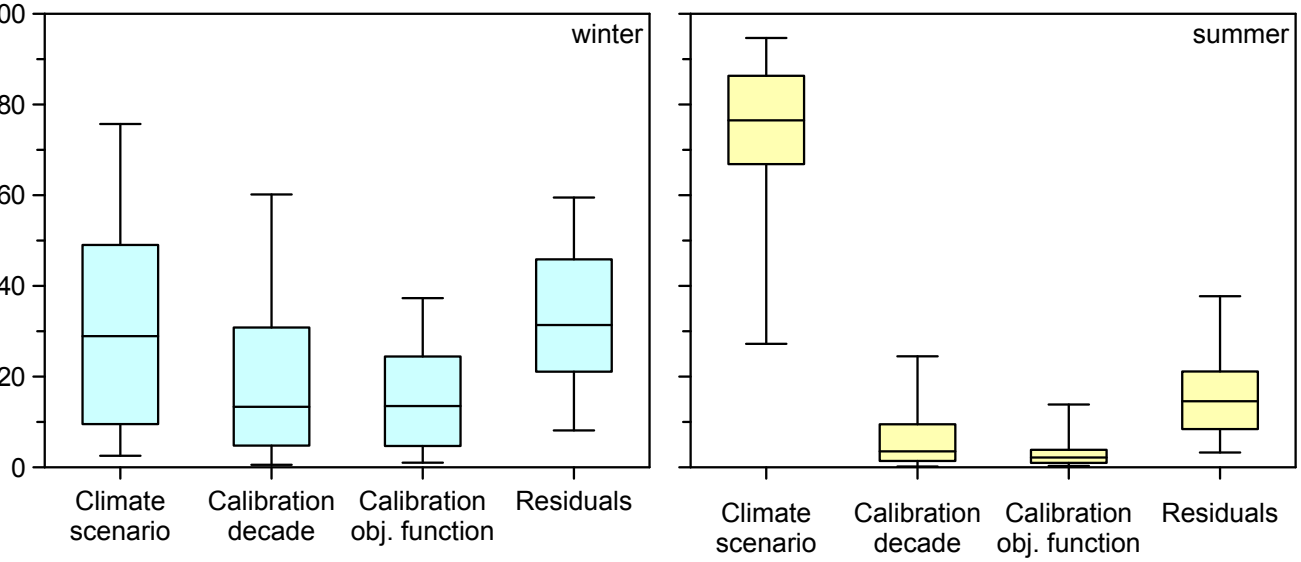
winter
summer
00
80
60
40
20
0
Climate scenario
Calibration decade
Calibration obj. function
Residuals
Climate scenario
Calibration decade
Calibration obj. function
Residuals